istered intravenously (0.3 mg/kg). After a bolus ICG injection, real-time imaging analysis was performed using an infrared camera and recorded with a digital camcorder for an optimized time. Our preliminary studies identified that ICG angiography in the hindlimbs initially revealed an angiogram, followed by a perfusion phase, when the fluorescence signals in the perfused tissue were simultaneously and homogeneously increased in both hindlimbs. After recording, the fluorescence intensity in the hindlimb was evaluated. Therefore, to evaluate perfusion in an ischemic hindlimb, the interested regions were selected from both right and left hindlimbs. The fluorescence signals of the left hindlimb in the perfusion phase were compared with those of the right, using NIH image software, and it revealed laterality in the ICG signal intensity. The time when the signal difference between the right and left was extremely evident was selected.

2.3. Evaluation of the relative blood flow using fluorescent microspheres

According to previous studies using fluorescent microspheres [15,16], we evaluated the relative blood flow between the left and right hindlimbs in mice. Briefly, after anesthesia, 200 μL of green FluoSphere fluorescent microspheres (15 μm, Molecular Probes, Invitrogen, Carlsbad, CA, USA) was administered within 1 min, followed by immediate sampling of blood and bilateral quadriceps femoris muscles. These samples were weighed accurately and incubated in 4 M KOH containing 2% of Tween 80 at 70 °C for 24 h. After measuring the fluorescence, the ratio of the fluorescence between the left and right hindlimbs, corrected by the tissue weight, was compared.

2.4. Thermography

One day after surgery, an initial temperature evaluation was performed in the hindlimbs using infrared thermography (MobIR M4 Thermal Camera, Wuhan Guide Infrared Technology Co., Ltd. China). The skin temperature of the mice under anesthesia was measured 3 times. Thereafter, for each mouse, temperature was evaluated 3 times by thermography during 4 weeks. The temperature distribution in the hindlimbs was compared between donepezil-treated and untreated mice and standardized by each non-ligated hindlimb as a reference. The laterality in temperature, represented by the ratio between the left and right hindlimb temperature, was evaluated.

2.5. Immunohistochemistry

The heart and quadriceps femoris muscle were excised and fixed in 4% paraformaldehyde. Some muscle samples were routinely

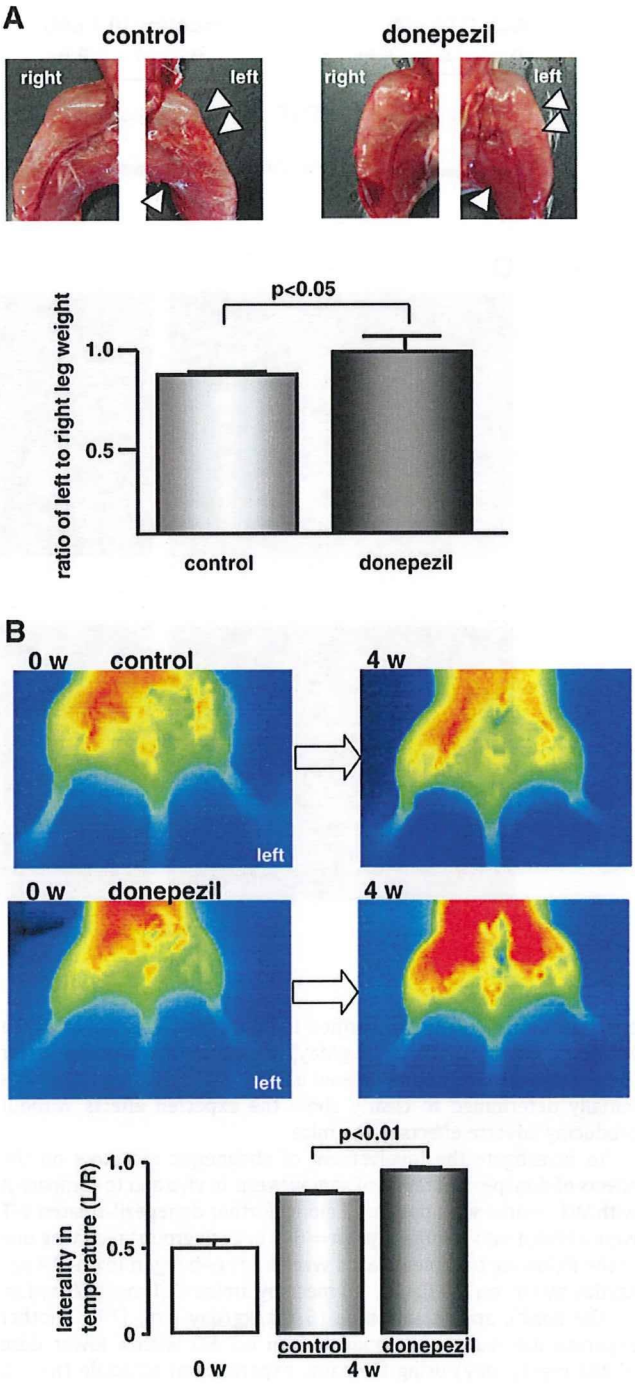

Fig. 2. Donepezil promotes angiogenesis in C57 BL6/J wild-type mice (WT) suffering from left hindlimb ischemia and suppresses ischemia-induced muscular atrophy and reduction of skin temperature. (A) WT treated with orally administered donepezil showed comparable muscular volume between the right and left hindlimb, even with the left hindlimb ischemia (arrowheads in the right panel), compared with untreated WT mice (arrowheads in the left panel) ($n=10$). (B) Donepezil accelerated skin temperature recovery in the left hindlimb within 4 weeks and sustained the skin temperature comparably to the right hindlimb. The ratio of skin temperature in the left hindlimb to the right, the laterality in the temperature, was increased by donepezil from 0.50 ± 0.04 after ligation to 0.95 ± 0.01 (vs. 0.81 ± 0.01 in control, $P<0.01$, $n=10$). (C) Compatible with this, donepezil-treated WT mice demonstrated more nuclei aligned with a vasculature-like appearance, especially in the left ischemic hindlimb (the right panel in donepezil, Fig. 2C). Magnification: ×200. Numbers of nuclei per visual field in the donepezil-treated left ischemic hindlimb increased significantly compared to the non-treated hindlimb ($P<0.01$, $n=9$). VEGF immunoreactivity was upregulated by donepezil in the left ischemic hindlimb (the right panel in Fig. 2C) compared with the control. Scale bars represent 50 μm. HIF-1α and VEGF protein expression in the left quadriceps femoris muscle increased significantly in donepezil-treated WT ($P<0.01$, $n=9$). (D) This effect of donepezil on VEGF signals did not significantly decrease following α-bungarotoxin, mecamylamine, or atropine treatment. Inhibition of caspase-3 by donepezil was also not attenuated by cholinergic antagonists. The PCNA expression level was elevated by donepezil but not reduced by α-bungarotoxin. (E) Donepezil increased VEGF and PCNA immunoreactivity, specifically in endothelial cells, whereas α-bungarotoxin did not affect VEGF- and PCNA-positive endothelial cells, as shown in the Western blot analysis. (F) Sustained skin temperature by donepezil was not blunted by α-bungarotoxin, mecamylamine, or atropine ($P<0.01$ vs. control, respectively). (G) ICG angiography revealed comparable tissue perfusion between the right and left hindlimbs in donepezil-treated WT (1.00 ± 0.84 vs. 1.08 ± 6.1; not significant, NS, $n=3$) (arrowheads in the right panel). In contrast, untreated WT mice showed lower tissue perfusion in the left hindlimb (0.74 ± 0.27 vs. 1.00 ± 0.43, $P<0.01$, $n=3$) (arrowheads in the left panel). Representative ICG angiography data from 3 experiments are presented. A microsphere assay also showed increased blood flow in donepezil-treated hindlimbs, evaluated with the ratio of left to right fluorescent signals (115.4 ± 19.3 in donepezil vs. 75.2 ± 7.5 in control, $P<0.05$, $n=5$).

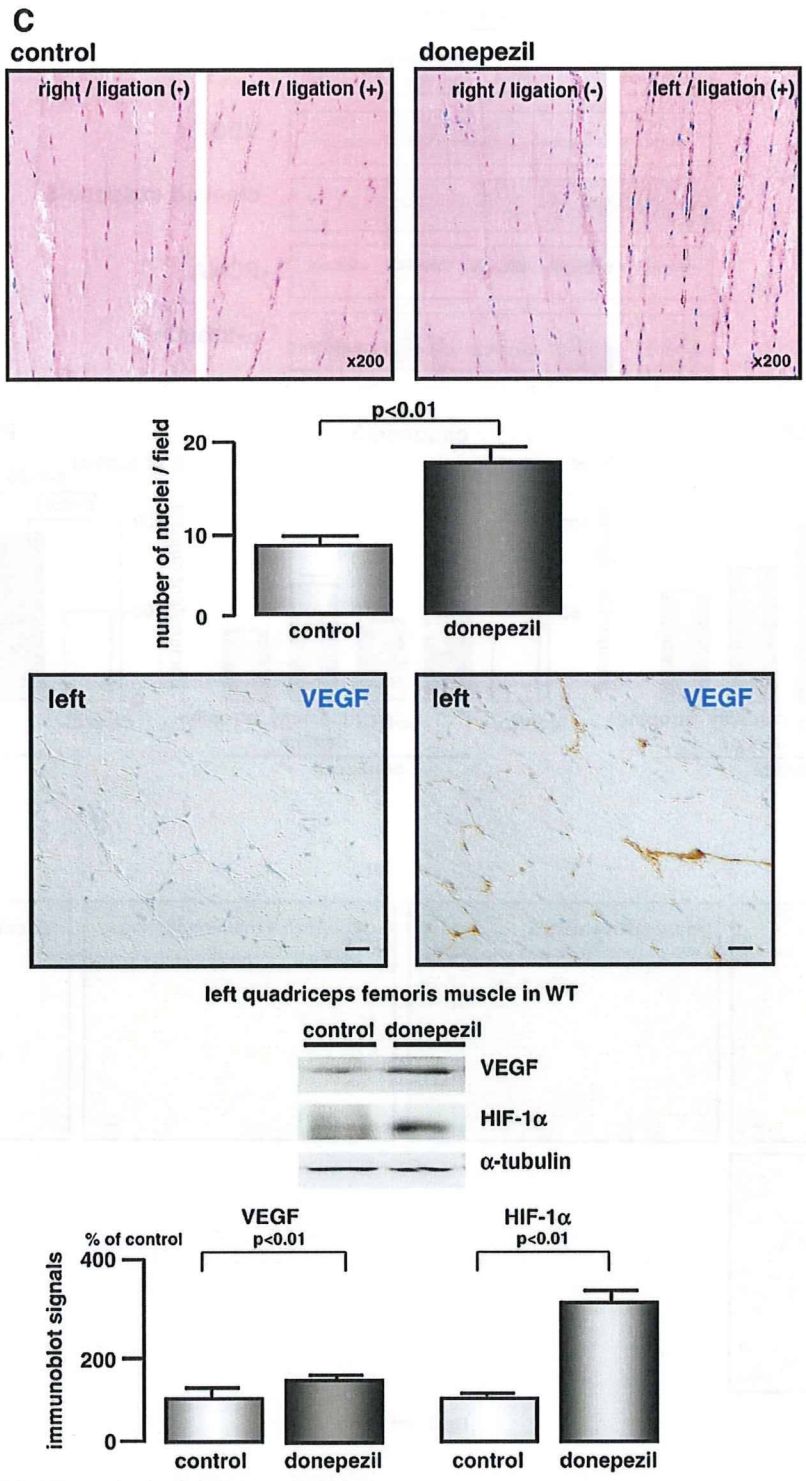

Fig. 2 (*continued*).

processed, paraffin-embedded, cut into 4-μm sections, and stained with hematoxylin and eosin. The number of nuclei in capillary-like structures per HPF were counted in randomly selected fields (9 fields per section). Other samples were used for immunohistochemical study using the Ventana automated immunohistochemistry system (Discovery TM, Ventana Medical System, Inc., Tucson, AZ, USA). Antigen retrieval was performed for 60 min in a preheated Dako Target Retrieval Solution (pH 6.0) using a microwave, followed by inhibition of intrinsic peroxidase, blocking, and the reaction with a primary antibody. VEGF and PCNA immunoreactivities were identified using a polyclonal anti-VEGF antibody at 1:100 (sc-152) (Santa Cruz Biotechnology, CA, USA) and a monoclonal anti-PCNA antibody at 1:2000 (Abcam Inc., Cambridge, MA, USA), respectively, based on the streptavidin–biotin–peroxidase reaction.

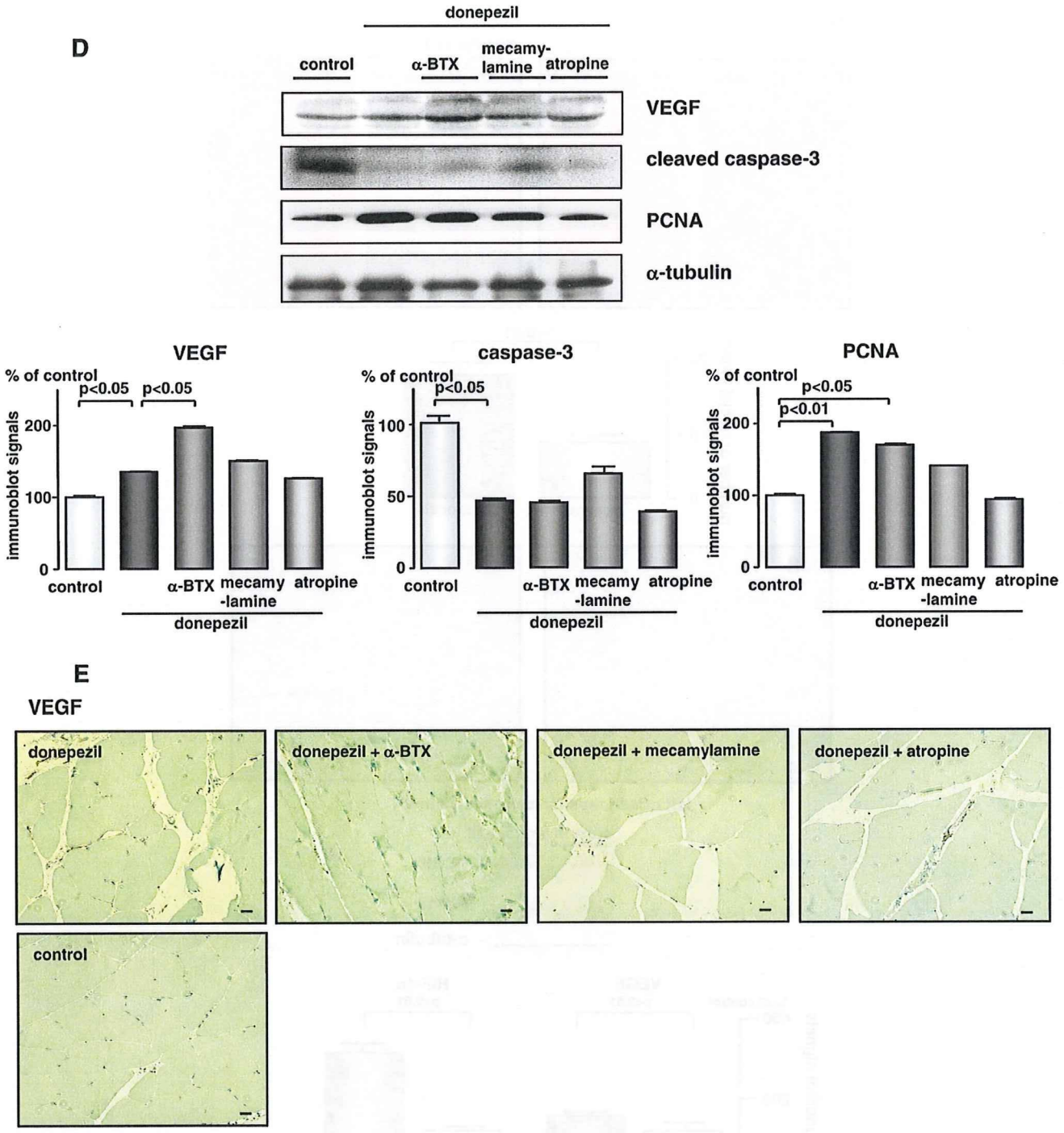

Fig. 2 (*continued*).

2.6. Western blotting

Whole muscle cell lysates were fractionated by SDS–PAGE and transferred onto membranes (Millipore Corp., Bedford, MA, USA). The membranes were incubated with polyclonal antibodies against VEGF (Santa Cruz Biotechnology), cleaved caspase-3 (Cell Signaling Technology, Danvers, MA, USA), diluted at 1:500, or with monoclonal antibodies against HIF-1α (Novus Biologicals, Inc., Littleton, CO, USA), pFlk-1 (Tyr 951, Santa Cruz Biochemistry), diluted at 1:500, α-tubulin (LAB VISION, Fremont, CA, USA), and PCNA (Abcam Inc.) diluted at 1:2000. Human umbilical vein endothelial cells (HUVECs), cultured in supplemented EGM-2 culture medium (Cambrex, Walkersville, MD, USA) on 24-well plates, were harvested with sample buffers. Similarly, the blotted membranes were incubated with a polyclonal anti-ChAT antibody (Millipore Corp., Bedford, MA, USA) diluted at 1:500, which detects several bands with an M.W. of 68–70 kDa. Each antibody was used in conjunction with a horseradish peroxidase-conjugated secondary antibody. For *in vitro* studies, each experiment was independently performed 3 times. After that, the densitometry analysis was performed.

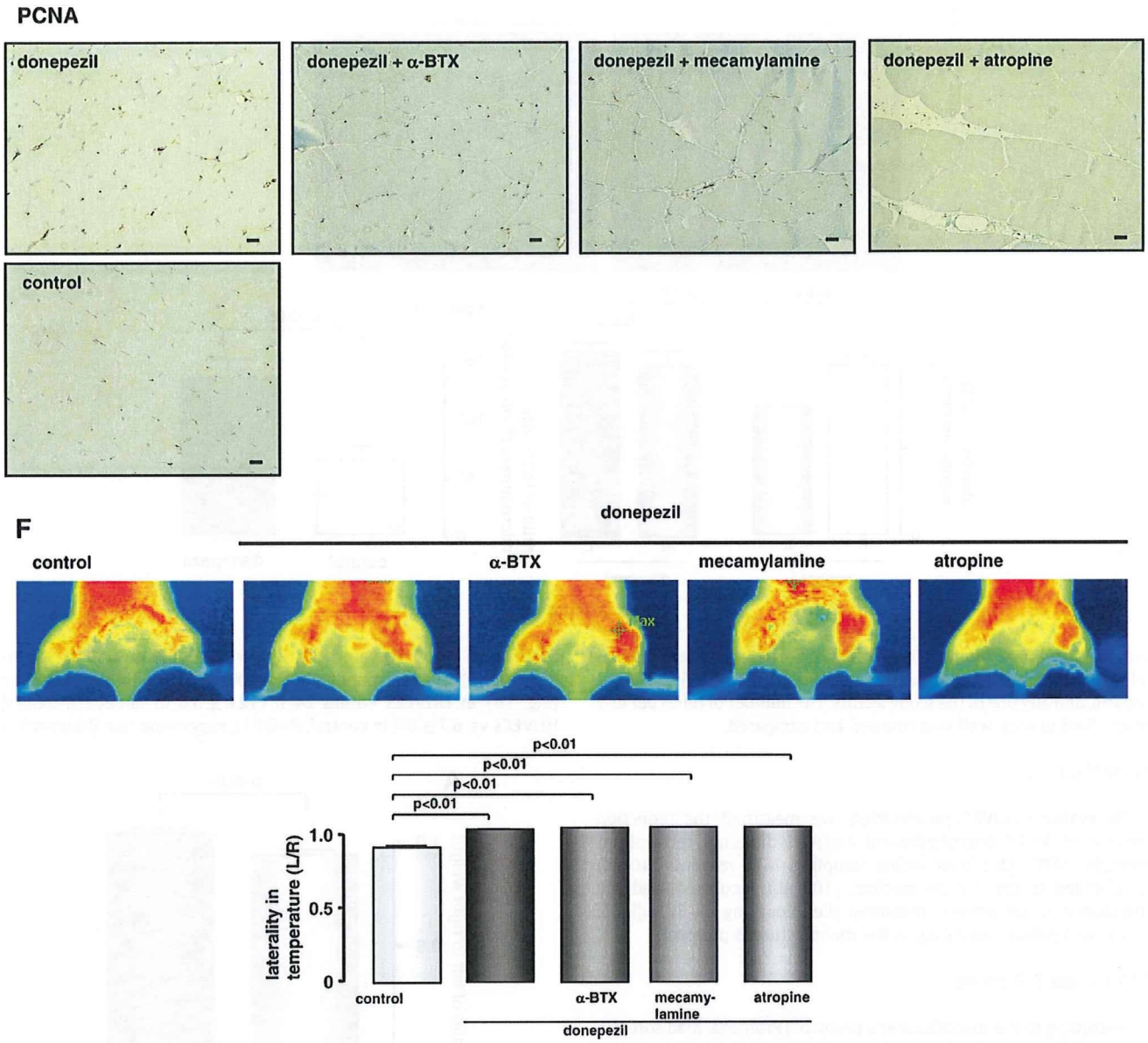

Fig. 2 (*continued*).

2.7. Reverse transcription-polymerase chain reaction (RT-PCR)

Total RNA was extracted from cells, and total RNA (1 μg) was reverse-transcribed to obtain single-stranded cDNA using a kit. Specific human cholinergic receptor primers were designed according to previous studies [17,18]. PCR amplification was performed with 40 cycles of the reaction and annealing temperatures of 60 °C. Primer sequences were as follows:

m1, TGAGGGCTCACCAGAGACT (forward),
GTCCAGGTGAGGATGAAGG (reverse);
m2, ACAAGGAAGGATAGTGAAGCC (forward),
CATCTCCATTCTGACCTGAAG (reverse);
α4, CTCACCGTCCTTCTGTGTC (forward),
CTGGCTTTCTCAGCTTCCAG (reverse);
α7, AGGCCACCTCATCAGCAG (forward),
GTACGCTGGTTTCCCTTTGA (reverse);
GAPDH, CGTCTTCACCACCATGGAGA (forward),
CGGCCATCACGCCACAGCTT (reverse).

2.8. Cell culture

HUVECs or human aorta endothelial cells (HAECs) were cultured in EGM-2 culture medium (Cambrex), supplemented with heparin, IGF-I, VEGF, bFGF, EGF, hydrocortisone, FBS, and ascorbic acid, according to the manufacturer's instruction. The final concentration of each reagent was as follows: 1 μM of donepezil (Eisai Co., Ltd., Tokyo, Japan), 0.1 μM of nicotine, which has been reported to possess angiogenic property [11-13], and 100 μM of ACh (Sigma-Aldrich, St. Louis, MO, USA).

To investigate the effects on tube formation, *in vitro* angiogenesis, HUVECs were cultured on Matrigel with complete growth factors (Becton Dickinson Labware, Bedford, MA, USA) using 96-well plates. HUVECs (1×10^4 cells) were seeded on Matrigel (50%)-coated wells

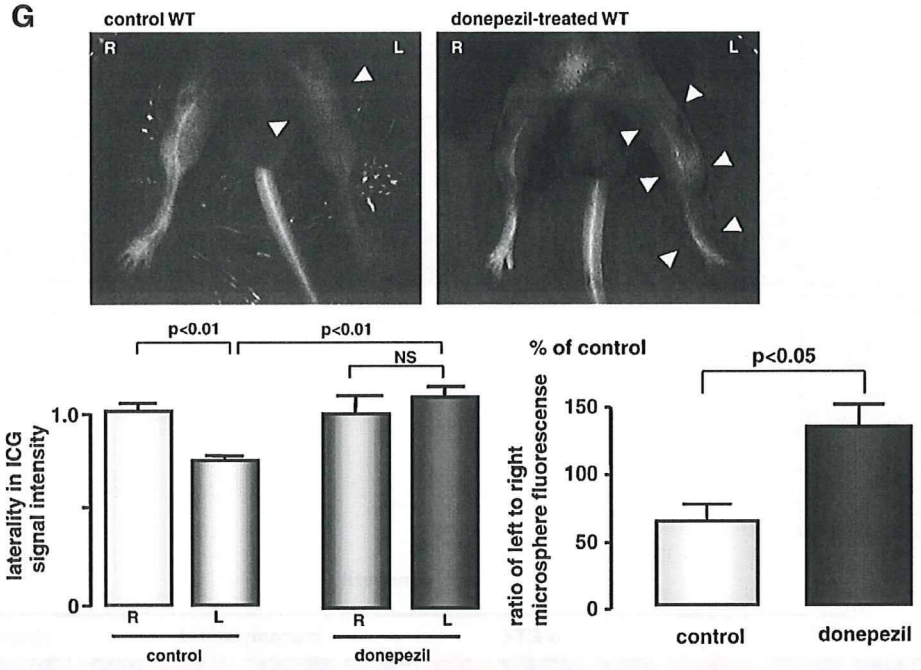

Fig. 2 (*continued*).

and incubated for 24 h in DMEM with 20% FBS, 25 μg/ml endothelial cell growth supplement (Upstate, Lake Placid, NY, USA), 10 U/ml heparin, and any one of the study agents. The number of tubes per low power field in each well was counted and compared.

2.9. MTT activity

To evaluate HUVEC proliferation, we measured the reduction activity of 3-(4,5-dimethylthiazol-2-yl)-2,5-diphenyl tetrazolium bromide (MTT). One hour before sampling, MTT reagents (10 μL) were added to the culture medium (100 μL), incubated, and the absorbance at 450 nm was measured (Cell Counting Kit-8; Dojindo, Kumamoto, Japan), according to the manufacturer's protocol.

2.10. Caspase 3/7 activity

According to the manufacturer's protocol (Promega, Madison, WI, USA), HUVECs treated with or without donepezil were cultured with an equal volume of Caspase-Glo 3/7 reagent for 3 h, followed by measuring the luminescence of each sample using the luminometer manufacturer's protocol.

2.11. Statistical analysis

The data are presented as means ± SE. The mean values between the 2 groups were compared using the unpaired Student's *t*-test. Differences among data for the in vitro studies were assessed by the Kruskal–Wallis test for multiple comparisons, followed by Scheffe's post-hoc test. Differences were considered significant at $P<0.05$.

3. Results

3.1. Donepezil activates angiogenic signals and accelerates tube formation in vitro

Donepezil transduces angiogenic signals. In the normoxic condition, donepezil (1 μM) elevated the HIF-1α protein level and then augmented expression of VEGF and activated phosphorylation of Flk-1, VEGF type 2 receptor (Fig. 1A), which composes critical angiogenic signaling. Correspondingly, donepezil enhanced tube formation (Fig. 1B) in HUVECs within 24 h (12.8 ± 0.6 in donepezil-treated HUVECs vs. 6.7 ± 0.4 in control, $P<0.01$), suggesting that donepezil is

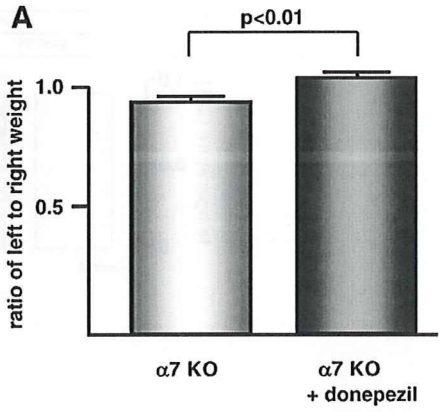

Fig. 3. Donepezil exhibits comparable angiogenic effects in the ischemic hindlimb model using α7 KO mice. (A) Donepezil inhibited ischemia-induced muscular atrophy in α7 KO. The ratio of the left leg weight to the right leg weight in donepezil-treated mice increased compared with untreated mice ($n=13$). (B) ICG angiography showed that donepezil attenuated ischemia-induced impairment of tissue perfusion (1.23 ± 0.10 vs. 0.70 ± 0.27, $P<0.01$, $n=3$) compared to untreated α7 KO. Representative ICG angiography data from 3 experiments are presented. Using a microsphere assay, donepezil inhibited the reduction of blood flow (117.4 ± 9.7 vs. 70.4 ± 10.7 in control, $P<0.05$, $n=5$ in each). (C) VEGF protein expression in the left ischemic hindlimb of donepezil-treated α7 KO increased compared with untreated α7 KO ($P<0.01$, $n=11$). More intense VEGF immunoreactivity was detected in donepezil-treated α7 KO, especially between each muscle fiber. Scale bar represents 50 μm. (D) Recovery of skin temperature in the left ischemic hindlimb of donepezil-treated α7 KO was more accelerated during the treatment (arrowheads in the lower panel). The laterality in temperature in α7 KO (0.71 ± 0.03), which was lower than that in WT (0.81 ± 0.02), increased with donepezil (0.98 ± 0.02, $P<0.01$, $n=13$). In contrast, untreated α7 KO showed poor skin temperature recovery (arrowheads in the upper panel). (E) Donepezil, even at a lower dose, inhibited the reduction in skin temperature in the left ischemic hindlimb (arrowheads in the lower panel), as evidenced by the elevation of laterality in temperature (0.96 ± 0.04, $P<0.01$, $n=9$).

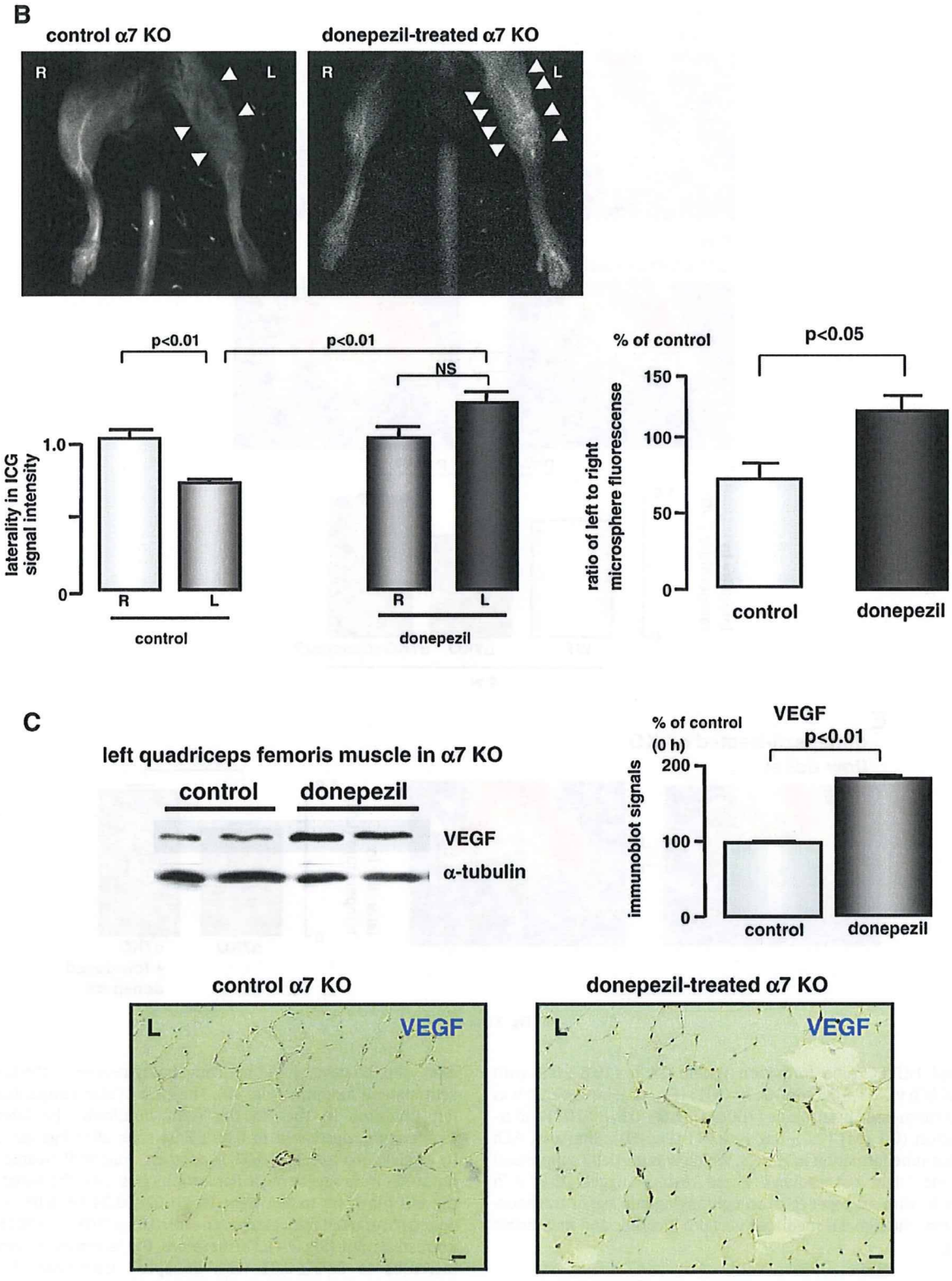

Fig. 3 (*continued*).

capable of accelerating angiogenesis. This effect of donepezil was inhibited by the muscarinic receptor antagonist atropine (100 μM) (0.7 ± 0.2, $P<0.01$) and the selective α7 nicotinic receptor antagonist α-bungarotoxin (0.1 μM) (2.0 ± 0.6, $P<0.01$) (Fig. 1B).

The mechanisms of donepezil-induced acceleration of angiogenesis were revealed by the effect of ACh as well as nicotine, which has been reported to promote angiogenesis [11-13], on HUVECs. ACh and nicotine shared the same angiogenic signals (Fig. 1C). Moreover, ACh

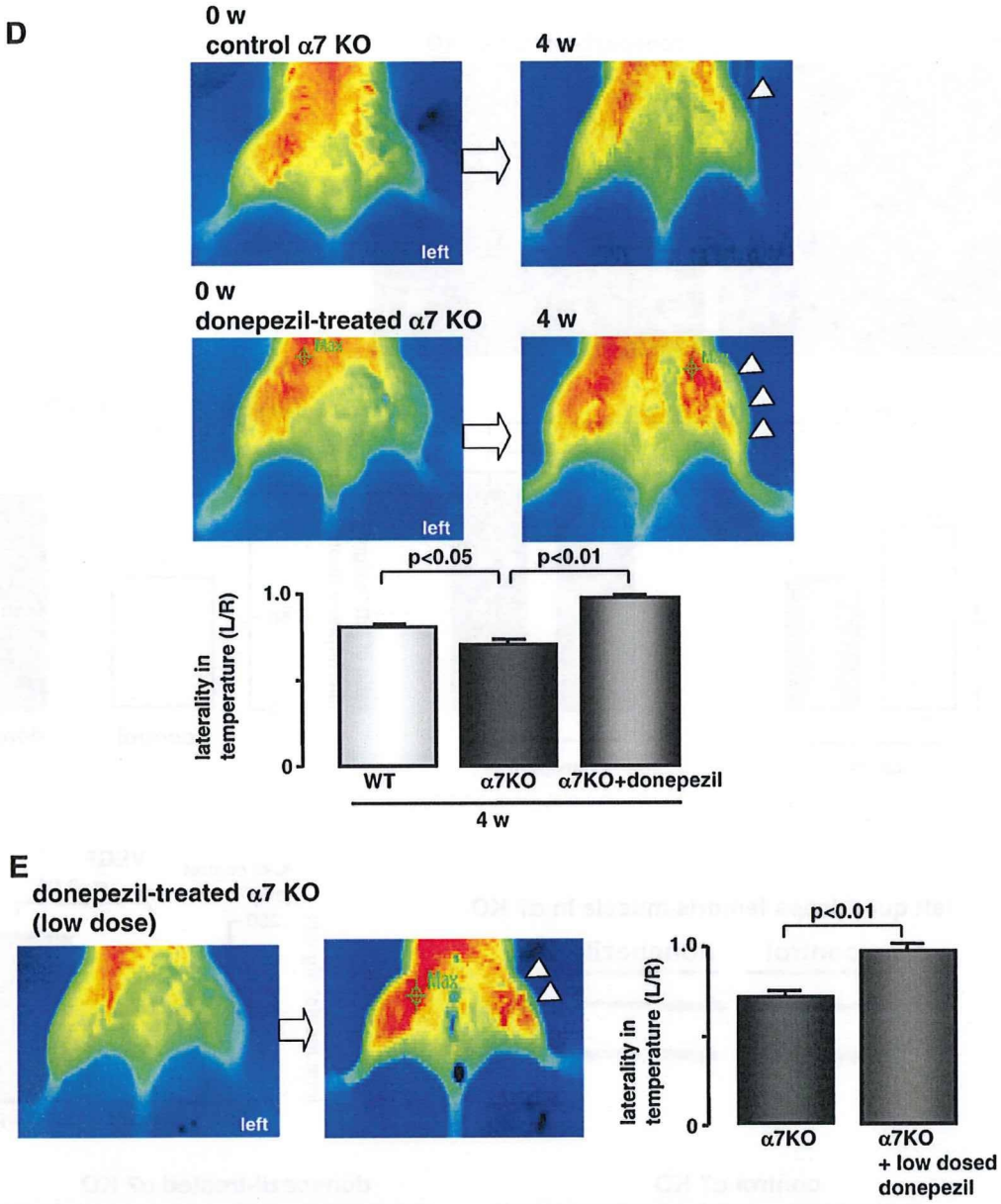

Fig. 3 (*continued*).

accelerated HUVEC tube formation within 24 h (16.8 ± 0.9 with 100 μM of ACh vs. 7.3 ± 0.5 control, $P<0.01$) (Fig. 1D); however, it was markedly suppressed by atropine (100 μM) (2.8 ± 0.8, $P<0.01$) and α-bungarotoxin (0.1 μM) (2.7 ± 0.6, $P<0.01$) (Fig. 1D). Similarly, ACh accelerated tube formation in HAECs, which was partially suppressed by atropine (data not shown). These results suggest that ACh promotes *in vitro* angiogenesis through angiogenic signal transduction and that the signal is mediated via both nicotinic and muscarinic receptors.

3.2. Donepezil promotes angiogenesis and suppresses ischemia-induced muscular atrophy in a murine hindlimb ischemia model

In untreated WT, muscular atrophy of the left quadriceps femoris muscle was evident within 4 weeks after hindlimb ischemia due to femoral artery ligation (Fig. 2A, arrowheads in the left panel). The temperature in the left ischemic limb increased gradually during the follow-up; however, it did not comparably recover to the level of the contralateral hindlimb (Fig. 2B). The ratio of skin temperature in the left hindlimb to that in the right hindlimb, the laterality in temperature, decreased to 0.50 ± 0.04 soon after ligation, followed by an elevation to 0.81 ± 0.02. In contrast, donepezil-treated mice did not suffer from severe muscular atrophy (Fig. 2A). The weight ratio of the left hindlimb to the right was 1.02 ± 0.04 ($P<0.05$, $n=10$) in donepezil-treated mice compared with 0.85 ± 0.01 ($n=10$) in control untreated mice (Fig. 2A). Furthermore, the laterality of temperature increased to 0.95 ± 0.01 with donepezil treatment ($P<0.01$ vs. control) (Fig. 2B). A pathological study revealed that, compared to untreated muscle (left in control, Fig. 2C), the number of nuclei in treated muscle increased along with more capillary-like structures (Fig. 2C). The number of nuclei per field in the donepezil-treated left hindlimb increased significantly compared to that in non-treated and ischemic hindlimbs (17.8 ± 1.4 vs. 8.6 ± 0.9, $P<0.01$, $n=9$). The immunohistochemical study showed that cells positive for

VEGF immunoreactivity were sparsely detected in the control. In contrast, dense VEGF signals were detected in the donepezil-treated muscle coincidence with small capillaries (Fig. 2C). Western blot analysis showed that the expression of both HIF-1α (318.4 ± 29.9 vs. 100.0 ± 6.7 in the control, $P<0.01$, $n=9$) and VEGF (144.5 ± 2.9 vs. 99.8 ± 9.9 in the control, $P<0.01$, $n=9$) in the left hindlimbs from donepezil-treated mice were higher than that in the left hindlimbs from the control (Fig. 2C).

These effects of donepezil were also evaluated using α-bungarotoxin, mecamylamine, and atropine (Fig. 2D). VEGF protein expression in the left hindlimb was elevated by donepezil ($P<0.05$); however, donepezil treatment combined with α-bungarotoxin did not suppress VEGF expression. Mecamylamine and atropine showed a trend toward reduced VEGF expression but could not diminish it completely (not significant vs. donepezil). Similarly, PCNA expression was elevated by donepezil ($P<0.01$), the level of which was not diminished by α-bungarotoxin ($P<0.05$); however, mecamylamine ($P<0.05$ vs. donepezil) and atropine ($P<0.01$ vs. donepezil) blunted PCNA expression. The VEGF and PCNA immunoreactive signals were especially localized at endothelial cells (Fig. 2E). Endothelial cells with both VEGF- and PCNA-positive signals were evident in left hindlimbs of donepezil-treated mice compared to those in controls. The protein level of cleaved caspase-3, an indicator of caspase-3 activation, was drastically reduced by donepezil ($P<0.05$) but was not affected by α-bungarotoxin, mecamylamine or atropine (not significant vs. donepezil). Furthermore, the laterality of temperature sustained by donepezil did not diminish with each antagonist ($P<0.01$ vs. control, but not significant vs. donepezil) (Fig. 2F). These results suggest that donepezil activates angiogenesis in a hindlimb ischemia model with upregulated angiogenic factors, enhanced proliferation, inhibition of apoptosis, and suppressed ischemia-induced muscular atrophy; however, partly not through already known cholinergic receptors.

Angiography with ICG revealed a marked increase in perfusion with donepezil treatment, which was comparable to the non-ischemic contralateral limb (1.08 ± 0.6 and 1.00 ± 0.84 vs. 0.74 ± 0.27, $P<0.01$). Furthermore, a blood flow assay using fluorescent microspheres revealed that donepezil enhanced blood flow recovery (124.9 ± 15.8 in donepezil vs. 59.0 ± 12.2 in control, $P<0.05$, $n=5$ in each) (Fig. 2G), suggesting that donepezil functionally recovered tissue perfusion in the ischemic hindlimb.

3.3. Donepezil accelerates angiogenesis even in α7 KO with hindlimb ischemia

Previous reports using α7 KO indicated that a nicotinic receptor is responsible for angiogenesis [11–13]. Therefore, to investigate whether the angiogenic effects of donepezil are mediated through α7 nicotinic receptors, we studied the effects of donepezil on peripheral limb ischemia using these mice. Compared with control untreated α7 KO (0.93 ± 0.02, $n=13$), donepezil-treated α7 KO surprisingly attenuated ischemia-induced muscular atrophy with a leg weight ratio of 1.01 ± 0.04 ($P<0.01$, $n=13$) (Fig. 3A). ICG angiography revealed that tissue perfusion in the left hidlimb was sustained in donepezil-treated α7 KO (1.23 ± 0.10 vs. 0.70 ± 0.27 in control, $P<0.01$), as supported by the microsphere assay (117.4 ± 9.7 vs. 70.4 ± 10.7 in control, $P<0.05$, $n=5$ in each) (Fig. 3B). VEGF expression in quadriceps femoris muscle from donepezil-treated α7 KO was more elevated (191.4 ± 10.0 vs. 100 ± 1.3 in control, $P<0.01$) (Fig. 3C) and the increased immunoreactivity was also detected in the treated muscle. Finally, donepezil accelerated temperature recovery in ischemic hindlimbs (Fig. 3D). Compared with the laterality in temperature in WT 4 weeks after ligation, that in α7 KO decreased further to 0.71 ± 0.03 (vs. 0.81 ± 0.02 in WT, $P<0.05$); however, treatment with donepezil elevated the ratio to 0.98 ± 0.02 even in α7 KO ($P<0.01$).

The lower dose of donepezil, 0.083 mg/kg/day, which is comparable to that used in clinical settings, was also effective for accelerating *in vivo* angiogenesis (the laterality in temperature 0.96 ± 0.04, $P<0.01$) (Fig. 3E). Taken with the *in vivo* data using α-bungarotoxin, these results also suggest that donepezil rescues ischemic hindlimbs independent of the α7 nicotinic receptor.

3.4. Donepezil augments VEGF expression in the heart and ChAT protein expression in endothelial cells

In addition to the ischemic hindlimb, donepezil also enhanced VEGF signals in the WT heart, compared to untreated WT (Fig. 4A), as supported by Western blot analysis (181.8 ± 4.2% vs. 100.0 ± 0.6% in control, $P<0.01$). Similar donepezil effects on VEGF production in the heart were observed in α7 KO (Fig. 4B). Compatible with VEGF immunoreactivity in the hindlimb, the immunohistochemical study with the anti-VEGF antibody showed positive signals with capillary-like appearance in the heart (Figs. 4A and B).

HUVECs were treated with 1 μM donepezil to study whether donepezil modulates ACh synthesis in endothelial cells. Donepezil elevated choline acetyltransferase (ChAT) protein expression in HUVECs (248.2 ± 3.1% vs. 100.0 ± 11.0% in control, $P<0.01$) (Fig. 4C). Because ChAT is a crucial enzyme for ACh synthesis, this suggests that donepezil regulates ACh level in endothelial cells. During treatment with donepezil, cholinergic receptor mRNAs in HUVECs were also upregulated. RT-PCR showed that m2, α4, and α7 mRNA expression were increased by donepezil, compared with α3 and GAPDH mRNA expression (Fig. 4D). Furthermore, in HUVECs treated with donepezil for 24 h, caspase 3/7 activity was suppressed when apoptosis was induced by growth factor withdrawal (69.3 ± 3.8% vs. control, $P<0.01$, $n=6$) (Fig. 4E). In contrast, donepezil showed only a trend toward increased MTT activity. Taken with the *in vivo* results, these in vitro data suggest that donepezil plays a role in inhibiting apoptosis and accelerating proliferation.

4. Discussion

The present study indicates 2 novel and critical points involved in an angiogenesis regulating system. First, ACh possessed angiogenic effects on endothelial cells, with increased HIF-1α expression, followed by elevated VEGF expression and accelerated tube formation, suggesting that ACh modulates intrinsic angiogenesis-responsible machinery in endothelial cells. Second, donepezil enhanced angiogenesis by activating the similar machinery. Specifically, donepezil activated protein expression of VEGF and ChAT, a critical enzyme for *de novo* ACh synthesis, accelerated endothelial cell proliferation, and inhibited apoptosis, partly independent of cholinergic receptors. These results suggest that donepezil regulates angiogenesis through a non-hypoxic HIF-1α induction pathway, which might be triggered by increased ACh [3,4].

Donepezil was developed to treat patients with Alzheimer's disease as an acetylcholinesterase inhibitor [12,13]. Donepezil prevents neurons from apoptosis and degeneration [19–22] and improves cognitive abilities in patients with Alzheimer's disease [23–25]. However, only few studies have focused on the angiogenesis-accelerating effects of donepezil [26]. Thus, the present study suggests a novel mechanism by which donepezil improves cognitive performance in these patients through acceleration of angiogenesis.

Our previous study demonstrated that ACh triggers a cell survival signal pathway and transactivates HIF-1α-regulated downstream genes, preventing cells from hypoxia-induced apoptosis [3]. This prompted us to speculate that cholinergic stimuli also possess angiogenesis-promoting effects. ACh clearly promoted angiogenesis and acceleration of tube formation; however, it is quite difficult to apply ACh directly to an *in vivo* model because ACh evokes life

threatening side effects, i.e., bronchospasm, enhanced secretion, and diarrhea [27,28]. Therefore, instead of ACh, we selected donepezil, which is globally used in clinical settings without side effects and has been demonstrated to increase tissue ACh levels [9,10,21]. As expected, donepezil promoted angiogenesis *in vitro* and concomitantly activated the HIF-1α/VEGF pathway. These effects of donepezil were also confirmed *in vivo*. Orally administered donepezil remarkably increased VEGF and PCNA immunoreactivity in endothelial cells of WT ischemic left quadriceps femoris muscles, indicating that donepezil activates angiogenesis by upregulating angiogenic signals in endothelial cells. To further study whether the effect of donepezil on endothelial cells is dependent on cholinergic receptors, donepezil treatment was conducted in the presence of each cholinergic receptor antagonist. Unexpectedly, *in vivo* angiogenesis was not clearly blunted by the antagonists, especially in terms of inhibiting apoptosis. α-Bungarotoxin, a selective α7 nicotinic receptor antagonist, did not inhibit apoptosis or expression of the angiogenic factors VEGF and PCNA, suggesting that donepezil plays an angiogenic role in endothelial cells independent of α7 nicotinic receptors. This result was also confirmed using α7 KO.

In this study, we used α7 KO to evaluate the *in vivo* angiogenic effects of donepezil. The studies by Cooke JP et al. utilizing α7 KO indicated that nicotine plays a crucial role in angiogenesis [11–13]. They demonstrated an impaired angiogenic effect of nicotine in α7

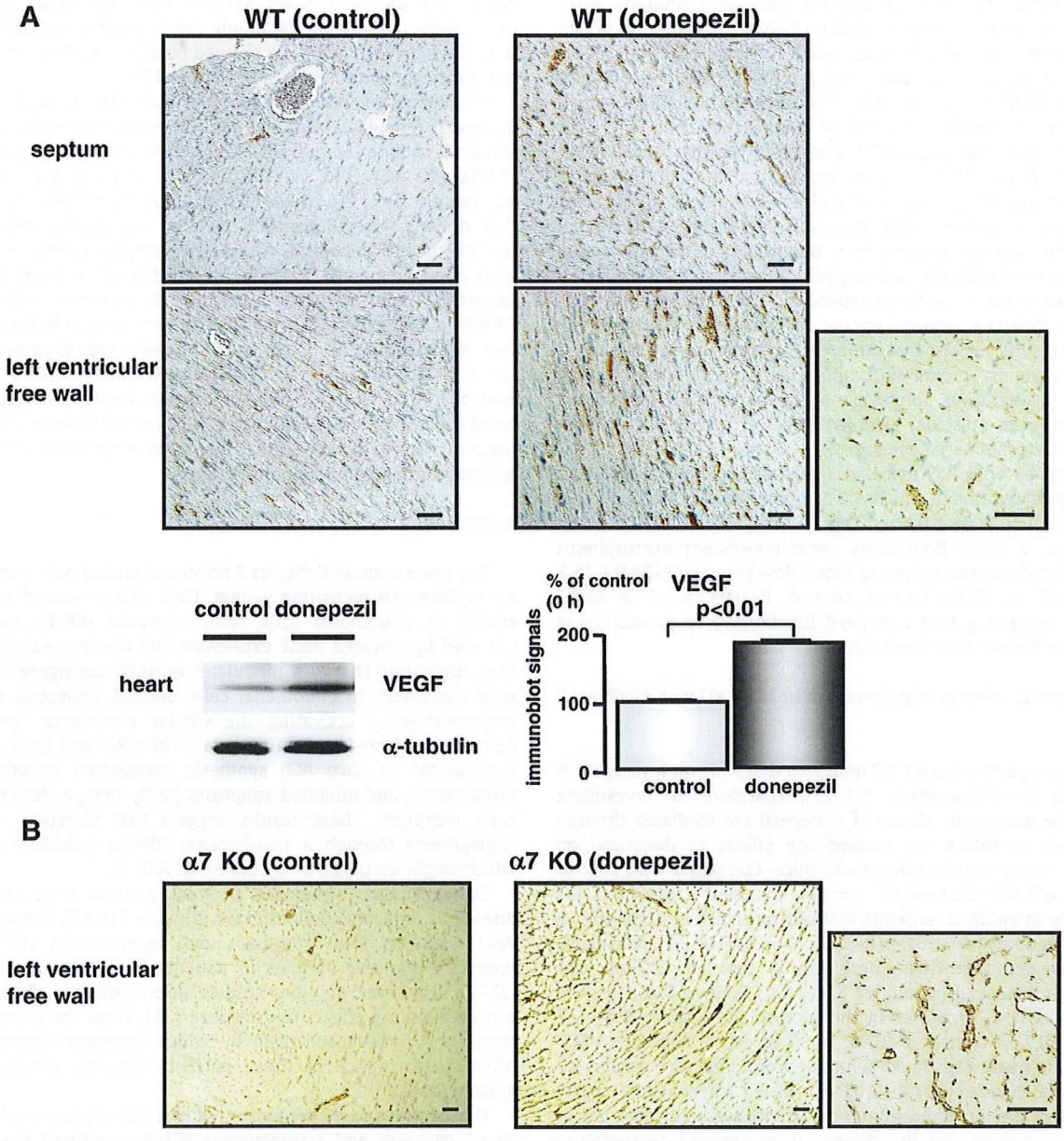

Fig. 4. Donepezil increases VEGF expression in the heart. (A) VEGF immunoreactivity was more in the heart of donepezil-treated WT than in that of untreated WT. Scale bars represent 50 μm. Cardiac expression of the VEGF protein was more enhanced by donepezil ($P<0.01$, $n=9$). (B) More VEGF-positive signals were also detected in donepezil-treated α7 KO than in untreated α7 KO. A magnified view is shown in panels A and B, which demonstrates the capillary-like appearance. Scale bars represent 50 μm. (C) Donepezil (1 μM) increased ChAT protein expression in HUVECs within 10 h ($P<0.01$, $n=6$). (D) mRNA expression of m2, α4, and α7 in HUVECs increased with donepezil within 24 h. In contrast, both α3 and GAPDH mRNA expression was not elevated. (E) Caspase 3/7 activity decreased significantly with a 24-h donepezil treatment (1 μM) in the case of depletion of growth factors (69.3 ± 3.8% vs. control, $P<0.01$, $n=6$); however, MTT activity was not affected by donepezil (NS).

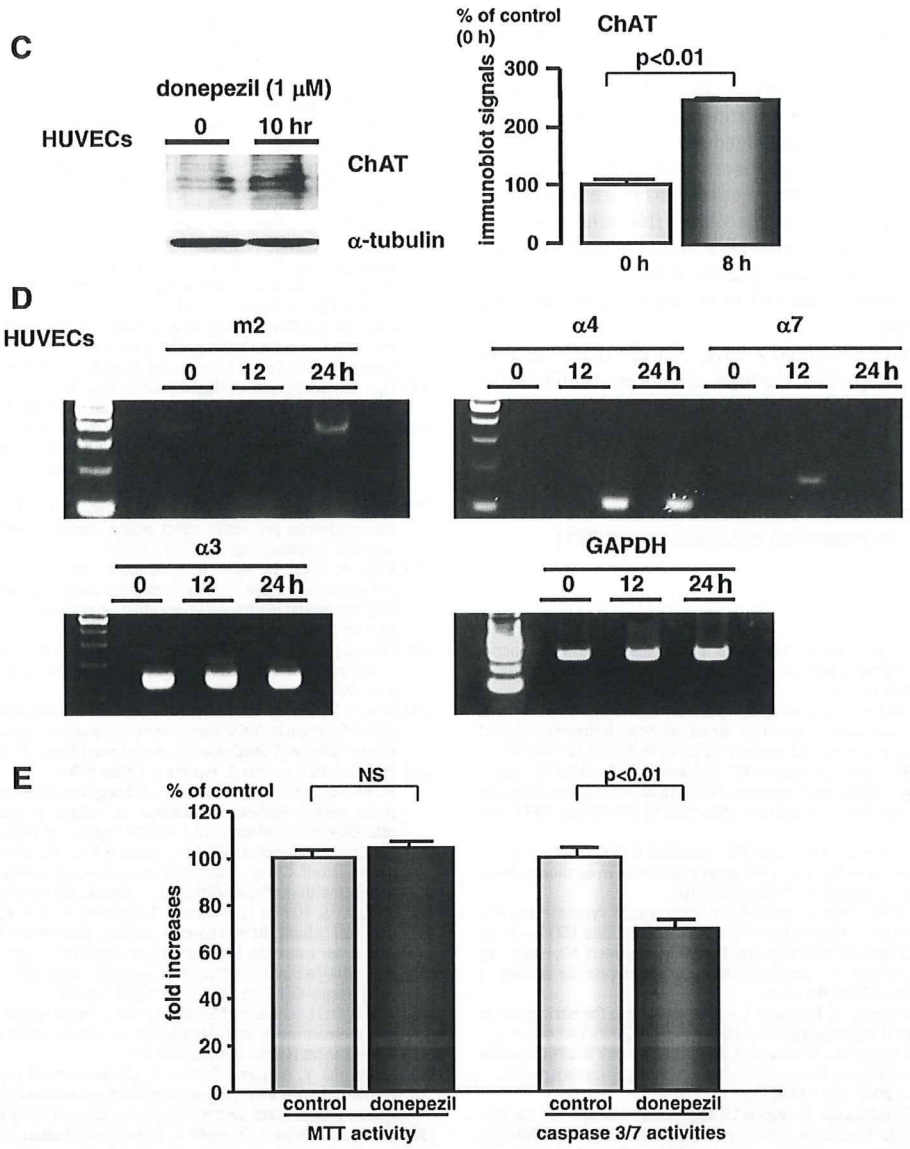

Fig. 4 (*continued*).

KO [12]. However, except for the α7 nicotinic receptor, there have been no studies investigating the role of cholinergic receptors involved in angiogenesis. Only α7 KO are available for angiogenesis studies; therefore, we selected them for the present study. Our results partially contrasted with Cooke's *in vitro* studies because the ACh effects were moderately blocked by both α-bungarotoxin and atropine, suggesting that the effects of ACh are mediated by 2 receptors, i.e., a nicotinic receptor and a muscarinic receptor. This discrepancy might be derived from different HUVEC sources used in the studies. We investigated the effects of donepezil using α7 KO expecting that the angiogenic effects of donepezil would be blunted. However, donepezil exhibited the angiogenesis-accelerating effect even in α7 KO. This result was also compatible with that of WT treated with donepezil and α-bungarotoxin. Taken with the WT results, this suggests that donepezil directly activates the angiogenic machinery and proliferation potency in endothelial cells, leading to inhibition of apoptosis, independent of α7 nicotinic receptors.

Because donepezil not only inhibits acetylcholinesterase but also upregulates ChAT, it was expected that the intracellular ACh level might be increased. However, even using HPLC, ACh levels could not be detected in endothelial cells, although we have thus far succeeded in measuring intracellular ACh levels of other cells, such as HEK293 cells, H9c2 cells, and primary rat cardiomyocytes [29]. This does not exclude the possibility that endothelial cells can synthesize ACh. As shown in this study, expression of other subtypes of cholinergic receptors, such as m2, α4, and α7, was upregulated by donepezil. This effect might also contribute to accelerated angiogenesis in α7 KO. The effects of donepezil on *in vivo* angiogenesis were also observed with a low dose, which is compatible with a clinical setting. Our preliminary study has already confirmed that a high dose of donepezil has no significant effects on murine heart rate or blood pressure. Therefore, it is suggested that low dose donepezil exerts angiogenic effect independent of hemodynamic effects.

Kawashima and Wessler [30,31] speculated that non-neuronal and non-central cells synthesize ACh. Our recent study has demonstrated for the first time that cardiomyocytes also possess the intracellular ACh synthesis system, which is transcriptionally activated in a positive feedback manner, and donepezil also elevates ACh level in cardiomyocytes, which was partly independent of muscarinic receptors [29]. These findings also suggest that donepezil exerts its own effects partly

independent of cholinergic receptors. On the basis of previous studies by Cooke, who did not clearly mention an ACh source, together with our recent study [29], it is suggested that systemically administered donepezil modulates ACh levels in various cells through a cholinergic receptor-dependent or -independent manner, and ACh derived from such cells might play a key role in angiogenesis.

Although donepezil is an acetylcholinesterase inhibitor, a lack of information on its receptor and action mechanisms makes our results difficult to interpret. Therefore, it is speculated that other mechanisms, i.e., a pathway other than acetylcholinesterase inhibition, might be involved in the angiogenesis-accelerating effects, and donepezil might directly bind to endothelial cell receptors not yet identified. This remains to be clarified.

In conclusion, we have presented a novel concept that donepezil possesses angiogenic properties through enhanced proliferation, increased angiogenic factor expression, and inhibition of apoptosis.

Acknowledgement

This study was supported by a Grant-in-Aid for Scientific Research from Japan Society for the Promotion of Science (19590251).

References

[1] Li M, Zheng C, Sato T, Kawada T, Sugimachi M, Sunagawa K. Vagal nerve stimulation markedly improves long-term survival after chronic heart failure in rats. Circulation 2004;109:120–4.
[2] Ando M, Katare RG, Kakinuma Y, Zhang D, Yamasaki F, Muramoto K, Sato T. Efferent vagal nerve stimulation protects heart against ischemia-induced arrhythmias by preserving connexin43 protein. Circulation 2005;112:164–70.
[3] Kakinuma Y, Ando M, Kuwabara M, Katare RG, Okudela K, Kobayashi M, Sato T. Acetylcholine from vagal stimulation protects cardiomyocytes against ischemia and hypoxia involving additive non-hypoxic induction of HIF-1alpha. FEBS Lett 2005;579:2111–8.
[4] Kuwabara M, Kakinuma Y, Ando M, Katare RG, Yamasaki F, Doi Y, Sato T. Nitric oxide stimulates vascular endothelial growth factor production in cardiomyocytes involved in angiogenesis. J Physiol Sci 2006;56:95–101.
[5] Zhao X, Lu X, Feng Q. Deficiency in endothelial nitric oxide synthase impairs myocardial angiogenesis. Am J Physiol Heart Circ Physiol 2002;283:H2371–2378.
[6] Ng QS, Goh V, Milner J, Stratford MR, Folkes LK, Tozer GM, Saunders MI, Hoskin PJ. Effect of nitric-oxide synthesis on tumour blood volume and vascular activity: a phase I study. Lancet Oncol 2007;8:111–8.
[7] Williams JL, Cartland D, Hussain A, Egginton S. A differential role for nitric oxide in two forms of physiological angiogenesis in mouse. J Physiol 2006;570:445–54.
[8] Ridnour LA, Isenberg JS, Espey MG, Thomas DD, Roberts DD, Wink DA. Nitric oxide regulates angiogenesis through a functional switch involving thrombospondin-1. Proc Natl Acad Sci U S A 2005;102:13147–52.
[9] Bohnen NI, Kaufer DI, Hendrickson R, Ivanco LS, Lopresti BJ, Koeppe RA, Meltzer CC, Constantine G, Davis JG, Mathis CA, Dekosky ST, Moore RY. Degree of nhibition of cortical acetylcholinesterase activity and cognitive effects by donepezil treatment in Alzheimer's disease. J Neurol Neurosurg Psychiatry 2005;76:315–9.
[10] Hatip-Al-Khatib I, Iwasaki K, Yoshimitsu Y, Arai T, Egashira N, Mishima K, Ikeda T, Fujiwara M. Effect of oral administration of zanapezil (TAK-147) for 21 days on acetylcholine and monoamines levels in the ventral hippocampus of freely moving rats. Br J Pharmacol 2005;145:1035–44.
[11] Heeschen C, Jang JJ, Weis M, Pathak A, Kaji S, Hu RS, Tsao PS, Johnson FL, Cooke JP. Nicotine stimulates angiogenesis and promotes tumor growth and atherosclerosis. Nat Med 2001;7:833–9.
[12] Heeschen C, Weis M, Aicher A, Dimmeler S, Cooke JP. A novel angiogenic pathway mediated by non-neuronal nicotinic acetylcholine receptors. J Clin Invest 2002;110:527–36.
[13] Heeschen C, Weis M, Cooke JP. Nicotine promotes arteriogenesis. J Am Coll Cardiol 2003;41:489–96.
[14] Li XW, Wang H. Non-neuronal nicotinic alpha7 receptor, a new endothelial target for revascularization. Life Sci 2006;78:1863–70.
[15] Cardinal TR, Hoying JB. A modified fluorescent microsphere-based approach for determining resting and hyperemic blood flows in individual murine skeletal muscles. Vascular Pharmacol 2007;47:48–56.
[16] Hodeige D, de Pauw M, Eechaute W, Weyne J, Heyndrickx GR. On the validity of blood glow measurement using colored microspheres. Am J Physiol Heart Circ Physiol 1999;276:H1150–1158.
[17] Elhusseiny A, Cohen Z, Olivier A, Stanimirović DB, Hamel E. Functional acetylcholine muscarinic receptor subtypes in human brain microcirculation: identification and cellular localization. J Cereb Blood Flow Metab 1998;19:794–802.
[18] Lips KS, Bruggman D, Pfeil U, Vollerthun R, Grando SA, Kummer W. Nicotinic acetylcholine receptors in rat and human placenta. Placenta 2005;26:735–46.
[19] Takada Y, Yonezawa A, Kume T, Katsuki H, Kaneko S, Sugimoto H, Akaike A. Nicotinic acetylcholine receptor-mediated neuroprotection by donepezil against glutamate neurotoxicity in rat cortical neurons. J Pharmacol Exp Ther 2003;306:772–7.
[20] Kimura M, Komatsu H, Ogura H, Sawada K. Comparison of donepezil and memantine for protective effect against amyloid-beta(1-42) toxicity in rat septal neurons. Neurosci Lett 2005;391:17–21.
[21] Kasa P, Papp H, Kasa Jr P, Torok I. Donepezil dose-dependently inhibits acetylcholinesterase activity in various areas and in the presynaptic cholinergic and the postsynaptic cholinoceptive enzyme-positive structures in the human and rat brain. Neuroscience 2000;101:89–100.
[22] Ginestet L, Ferrario JE, Raisman-Vozari R, Hirsch EC, Debeir T. Donepezil induces a cholinergic sprouting in basocortical degeneration. J Neurochem 2007;102:434–40.
[23] Rogers SL, Doody RS, Mohs RC, Friedhoff LT. Donepezil improves cognition and global function in Alzheimer disease: a 15-week, double-blind, placebo-controlled study. Donepezil Study Group. Arch Intern Med 1998;158:1021–31.
[24] Feldman H, Gauthier S, Hecker J, Vellas B, Xu Y, Ieni JR, Schwam EM. Donepezil MSAD Study Investigators Group. Efficacy and safety of donepezil in patients with more severe Alzheimer's disease: a subgroup analysis from a randomized, placebo-controlled trial. Int J Geriatr Psychiatry 2005;20:559–69.
[25] Gauthier S, Feldman H, Hecker J, Vellas B, Emir B, Subbiah P. Donepezil MSAD Study Investigators' Group. Functional, cognitive and behavioral effects of donepezil in patients with moderate Alzheimer's disease. Curr Med Res Opin 2002;18:347–54.
[26] Shimizu S, Hanyu H, Iwamoto T, Koizumi K, Abe K. SPECT follow-up study of cerebral blood flow changes during donepezil therapy in patients with Alzheimer's disease. J Neuroimaging 2006;16:16–23.
[27] Fryer AD, Jacoby DB. Muscarinic receptors and control of airway smooth muscle. Am J Respir Crit Care Med 1998;185:S154–60.
[28] Kavirajan H, Schneider LS. Efficacy and adverse effects of cholinesterase inhibitors and memantine in vascular dementia: a meta-analysis of randomised controlled trials. Lancet Neurol 2007;6:782–92.
[29] Kakinuma Y, Akiyama T, Sato T. Cholinoceptive and cholinergic properties of cardiomyocytes involving an amplification mechanism for vagal efferent effects in sparsely innervated ventricular myocardium. FEBS J 2009;276:5111–25.
[30] Fujii T, Tsuchiya T, Yamada S, Fujimoto K, Suzuki T, Kasahara T, Kawashima K. Localization and synthesis of acetylcholine in human leukemic T cell lines. J Neurosci Res 1996;44:66–72.
[31] Klapproth H, Reinheimer T, Metzen J, Munch M, Bittinger F, Kirkpatrick CJ, Hohle KD, Schemann M, Racke K, Wessler I. Non-neuronal acetylcholine, a signalling molecule synthezised by surface cells of rat and man. Naunyn Schmiedebergs Arch Pharmacol 1997;355:515–23.

OPEN ACCESS Freely available online

PLoS one

Engineered Heart Tissue: A Novel Tool to Study the Ischemic Changes of the Heart *In Vitro*

Rajesh G. Katare*¤, Motonori Ando, Yoshihiko Kakinuma, Takayuki Sato

Department of Cardiovascular Control, Kochi Medical School, Nankoku, Japan

Abstract

Background: Understanding the basic mechanisms and prevention of any disease pattern lies mainly on development of a successful experimental model. Recently, engineered heart tissue (EHT) has been demonstrated to be a useful tool in experimental transplantation. Here, we demonstrate a novel function for the spontaneously contracting EHT as an experimental model in studying the acute ischemia-induced changes in vitro.

Methodology/Principal Findings: EHT was constructed by mixing cardiomyocytes isolated from the neonatal rats and cultured in a ring-shaped scaffold for five days. This was followed by mechanical stretching of the EHT for another one week under incubation. Fully developed EHT was subjected to hypoxia with 1% O_2 for 6 hours after treating them with cell protective agents such as cyclosporine A (CsA) and acetylcholine (ACh). During culture, EHT started to show spontaneous contractions that became more synchronous following mechanical stretching. This was confirmed by the increased expression of gap junctional protein connexin 43 and improved action potential recordings using an optical mapping system after mechanical stretching. When subjected to hypoxia, EHT demonstrated conduction defects, dephosphorylation of connexin-43, and down-regulation of cell survival proteins identical to the adult heart. These effects were inhibited by treating the EHT with cell protective agents.

Conclusions/Significance: Under hypoxic conditions, the EHT responds similarly to the adult myocardium, thus making EHT a promising material for the study of cardiac functions in vitro.

Citation: Katare RG, Ando M, Kakinuma Y, Sato T (2010) Engineered Heart Tissue: A Novel Tool to Study the Ischemic Changes of the Heart *In Vitro*. PLoS ONE 5(2): e9275. doi:10.1371/journal.pone.0009275

Editor: Fabrizio Gelain, University of Milan-Bicocca, Italy

Received December 18, 2009; **Accepted** January 25, 2010; **Published** February 17, 2010

Funding: This study was supported by a Health and Labor Sciences Research Grant (H14-NANO-002, H16-NANO-005) from the Ministry of Health, Labor, and Welfare of Japan, and by a Grant-in-Aid for Scientific Research (15300165, 17790892) from the Ministry of Education, Science, Sports, and Culture of Japan. The funders had no role in study design, data collection and analysis, decision to publish, or preparation of the manuscript.

Competing Interests: The authors have declared that no competing interests exist.

* E-mail: katarerajesh@yahoo.com

¤ Current address: Bristol Heart Institute, University of Bristol, Bristol, United Kingdom

Introduction

Understanding the basic mechanisms and prevention of any disease pattern lies mainly on development of a successful experimental model. Tissue engineering is a newly developed technique that comprises of constructing a three dimensional structure from cardiomyocytes or progenitor cells and transplanting them in to in vivo reconstruction of the diseased myocardium [1,2,3,4,5,6]. While all the studies have used EHT as a therapeutic tool, it not known if EHT can also replace the whole heart to study the characteristics of cardiovascular diseases in vitro, although Zimmermann and colleagues suggested that EHT could become a promising material to study cardiac functions in vitro [4]. Recent development of vascularized EHT [7,8,9] further supports our hypothesis that EHT could become a replacement for whole heart studies under in vitro circumstances. In this study, using advanced techniques of optical mapping along with other conventional techniques, we demonstrate that EHT responds similar to the whole heart under basal and stress conditions.

Methods

One to three days old neonatal rats born to female Wistar rats (SLC, Japan) were used. All animals received humane care in compliance with the "Guide for the Care and Use of Laboratory Animals" prepared by the Institute of Laboratory Animal Resources and published by the National Institute of Health (NIH Publication No. 86–23, revised 1985) and approved by the ethical committee of Kochi Medical School, Japan.

Cell Isolation

Cardiomyocytes were isolated from neonatal Wistar rats (postnatal day 1 to 3) by a fractionated DNase/Trypsin digestion protocol as described earlier [1]. The resulting cell population (50% cardiomyocytes/50% nonmyocytes [3]) was immediately subjected to EHT generation.

Construction of EHT

EHTs were constructed as described previously. [4] Briefly, acetic acid solubilized collagen type I was mixed with concentrated

culture medium (2× DMEM, 20% horse serum, 4% chick embryo extract, 200 U/mL penicillin, 200 μg/mL streptomycin). The pH was neutralized by titration with 0.1 N NaOH. Matrigel was added (10% v/v) if indicated. Finally, cells were added to the reconstitution mixture, which was thoroughly mixed before casting in circular molds (inner diameter, 5 mm; outer diameter, 10 mm; height, 5 mm). Within 3 to 5 days, EHT coalesced to form spontaneously contracting circular structures and were transferred on automated stretch devices conventionally constructed in our laboratory (**Fig 1 and Video S1**).

Hypoxia – Reoxygenation

To understand if fully developed EHT behaves similar to adult myocardium under stress, we used hypoxia-reoxygenation to simulate myocardial ischemia-reperfusion in vivo. For this purpose, the spontaneously contracting EHT was subjected to 6 h of hypoxia by culturing them with 1% O_2 followed by 12 h of reoxygenation. At the end of experimental protocol the EHT was randomly assigned to undergo optical mapping to study the changes in conduction velocity or for protein extraction to study the changes in pro-survival signaling cascade.

To demonstrate if the EHT could exhibit similar responses of the adult heart to treatment with pharmacological agents under hypoxic stresses, the EHT was treated with cyclosporin (CsA, 0.2μM) or acetylcholine (ACh, 500μM) before hypoxia. We and others [10,11,12,13] have previously demonstrated the cytoprotective effects of CsA or ACh on myocardium after acute ischemic injury (**Fig 1**).

Optical Mapping

EHTs were superfused with warmed Tyrode's solution (135 mM NaCl, 5.4 mM KCl, 1.8 mM $CaCl_2$, 1 mM $MgCl_2$, 0.33 mM NaH_2PO_4, 5 mM HEPES, and 5 mM glucose) containing the voltage-sensitive dye di-4-ANEPPS (10 μM; Molecular Probes, Eugene, OR). After 7 min, the chamber was sealed and the dye was washed out as described earlier [14]. Action potentials (AP) were optically mapped using a CMOS-based high speed and high resolution optical mapping system (MICAM ULTIMA, Brainvision, Japan).

Protein Preparation and Immunoblotting

As described previously [11,15] the samples obtained at the end of experiments were prepared for immunoblot analysis. Extracted proteins were quantified with a BCA Assay Kit (Sigma). Equal amounts of proteins (50μg of total protein) were separated by SDS-PAGE, and transferred to a PVDF membrane (Millipore). After blocking nonspecific sites with 5% non-fat milk in TBS supplemented with 0.1% Tween20 over night, the membranes were probed with primary antibodies against Connexin 43 (1:1000, Zymed Laboratories), Akt (1:1000, Cell Signaling) and phospho Akt (1:1000, Cell Signaling), BCl-2 (1:1000, Cell Signaling), and α-sarcomeric actin (1:1000, Abcam). Beta-actin (1:1000, Cell Signaling) was used as loading control of the protein samples. Anti-rabbit IgG conjugated with horseradish peroxidase (diluted 1:5000, Santa Cruz) was used as secondary antibodies and the membranes were finally developed with an ECL chemiluminescence reagent (Amersham). The samples were quantified by densitometry using Kodak Gel Logic 100 system (Kodak, Japan).

Electron Microscopy

Following different protocols, the EHTs were divided into approximately 1 mm blocks and immediately fixed with cold 2% glutraldehyde. After 24 hr fixation at 4°C the samples were postfixed with 1% osmium tetroxide for 1 hr, dehydrated with increasing concentrations of alcohol (50%, 70%, 80%, 90%, and 100%; three times at each concentration) for 10 min each. Next, cells were infiltrated with propylene oxide for 15 min, followed by 1:1 propylene oxide: epoxy resin for 4 hr. Samples were then embedded with fresh epoxy resin into molds and placed in an 80°C oven for 18 hr. Ultrathin sections were stained with uranyl acetate and lead citrate and were examined under an electron microscope [16].

Statistical Analysis

Differences between two groups were analyzed using t-test (paired or unpaired as appropriate). Values are expressed as

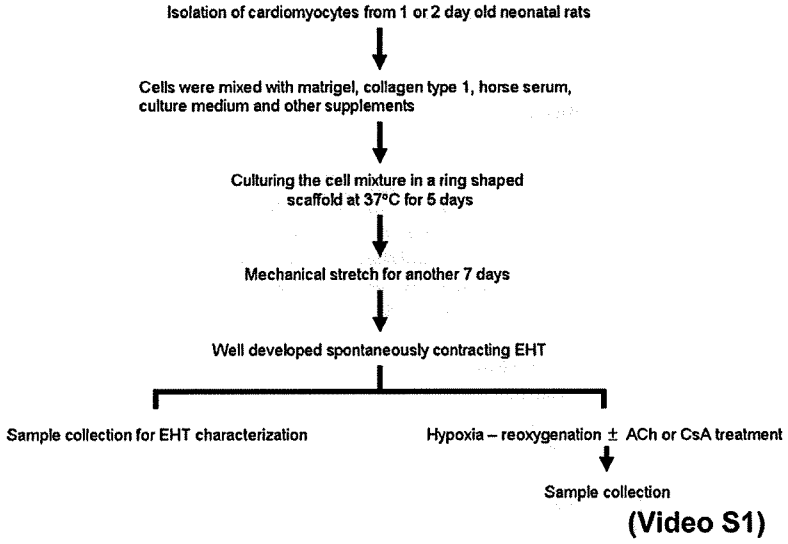

Figure 1. Experimental Protocol. Experimental protocol of the study.
doi:10.1371/journal.pone.0009275.g001

mean±SD. A P value of <0.05 was considered statistically significant for all parameters.

Results

Construction of Functionally Active EHTs

Using the whole cell population from neonatal hearts we successfully constructed functionally active EHTs (**Video S1**). At day 5 after culture, the EHT demonstrated irregular fibrillation like contractions which became synchronous and regular after mechanical stretching (**Video S1**). The functionality of the constructed EHT was confirmed first using electron microscopy, showing fully developed adult cardiomyocytes with normally arranged sarcomeres (**Fig 2A**). Immunoblotting confirmed the expression of cardiac specific connexin 43 and α-sarcomeric actin (**Fig 2B**). Most importantly, mechanical stretches resulted in upregulation of these proteins (**Fig 2B**). Further, optical mapping showed synchronic conduction velocity as measured by the action potential recording across constructed EHTs (**Fig S1 and Fig 2C**).

EHT Responds to Hypoxic Stresses

Next we tested if the constructed EHT could respond to hypoxic stress in a similar way to the whole heart. For this purpose, the EHTs were subjected to hypoxia and reoxygenation to simulate myocardial ischemia in vitro. Similar to the adult heart [12], hypoxia induced dephosphorylation of gap junctional protein connexin 43 (**Fig 3A**) and loss of normal conduction across EHT (**Fig 3B**). This was further confirmed by the molecular analysis of cell survival Akt and Bcl-2, both of which were downregulated in EHT subjected to hypoxia (**Fig 4**). Most importantly, treating EHT with pro-survival ACh or CsA [10,16], markedly inhibited the hypoxia induced damage to the EHT ($P<0.01$, **Fig 3 and 4**).

Discussion

Cardiac tissue engineering is an emerging field that may hold great promise for advancing the treatment of heart diseases [17]. EHTs have been developed in the view of myocardial

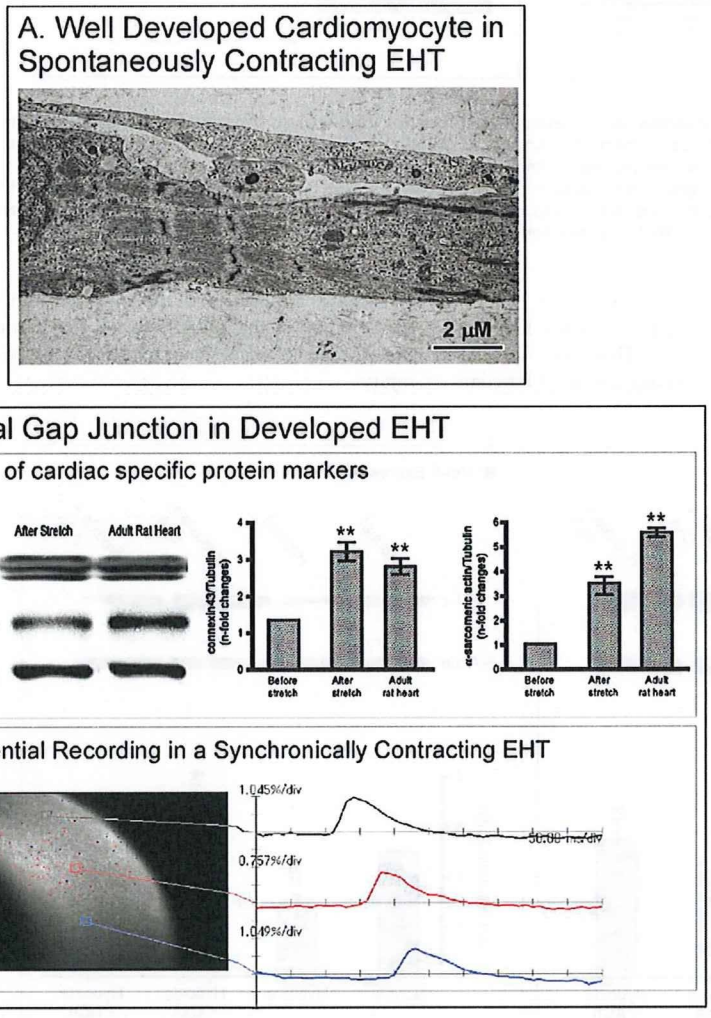

Figure 2. Characterization of the fully developed EHT. Samples were collected for electron microscopy (A) and western blotting (B1) after mechanical stretching. Tubulin was used as a loading control. Densitometry analysis was perfomed as explained in the methods. **P<0.001 versus before stretch. For optical mapping (B2), The EHT was loaded with voltage sensitive dye and images were captured with a CMOS-based high speed and high resolution optical mapping system.
doi:10.1371/journal.pone.0009275.g002

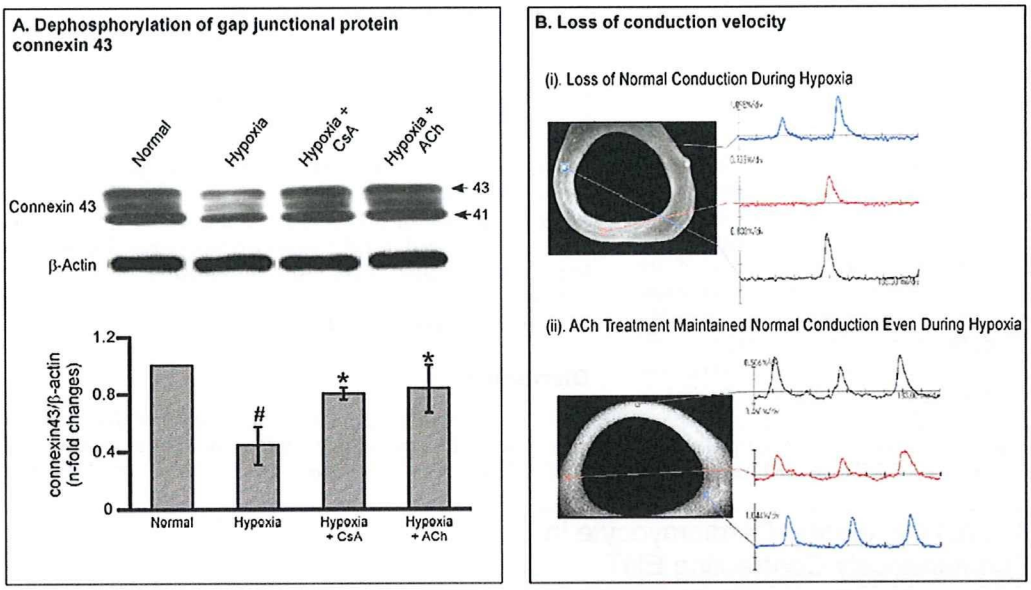

Figure 3. Response of EHT to hypoxic stress. A. Representative Immunoblotting analysis of connexin 43 in EHTs subjected to hypoxic stresses. Arrows indicate positions of phosphorylated isoform of connexin 43 (43 kDa) and nonphosphorylated isoform of connexin 43 (41 kDa) bands, respectively. Quantitative densitometric analysis represents the phosphorylated isoform of connexin 43. Values are mean ± SD $^{\#}P<0.05$ versus normal group and $^{*}P<0.05$ versus hypoxic group. N = 5 in each group. **B.** Representative images showing the conduction defect evaluated by optical mapping, following exposure of EHTs to hypoxia, which was reverted by treatment with ACh. The synchronous conduction was lost in the EHT subjected to hypoxia. However, treatment with ACh prevented the conduction defect.
doi:10.1371/journal.pone.0009275.g003

replacement therapy [1,2,5,8] and several studies have demonstrated the feasibility of EHTs in improving the cardiac function following myocardial injury [18,19,20]. However, to our knowledge this is the first study demonstrating the novel function of EHTs as a replacement model to the whole heart, for studying the response of the heart to any form of stresses, and to screen the pharmacological compounds for treatment of myocardial injury.

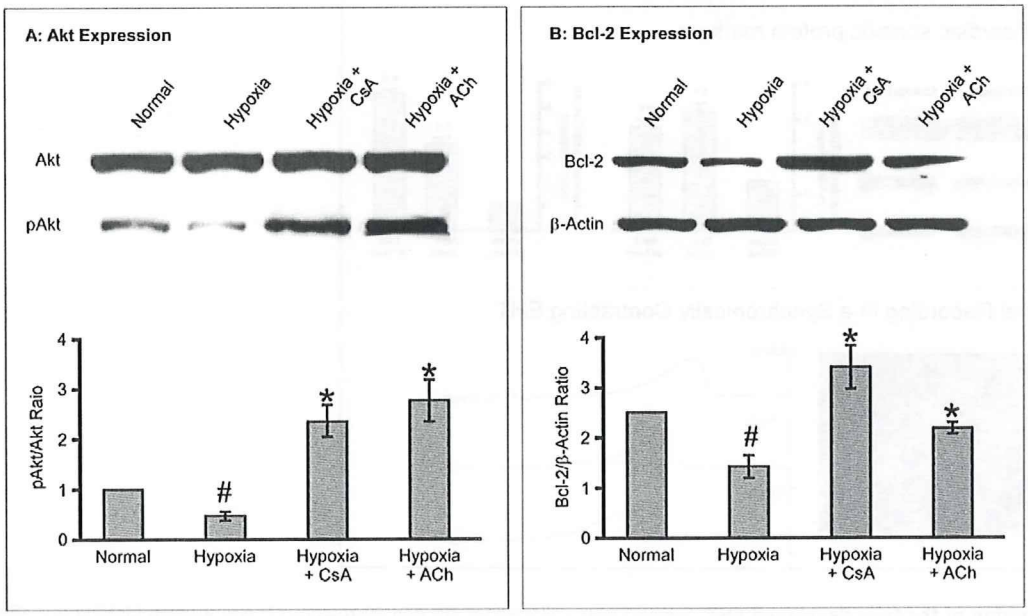

Figure 4. Cell survival Cascade analysis. Representative immunoblot and quantitative analysis of Akt (A) and Bcl-2 (B) in EHTs exposed to hypoxia. Values are mean ± SD $^{\#}P<0.05$ versus normal group and $^{*}P<0.05$ versus hypoxic group. N = 5 in each group.
doi:10.1371/journal.pone.0009275.g004

Understanding the basic mechanisms of diseases is accelerated by a good experimental model. Rodent models are widely used for the study of various cardiovascular diseases, especially to study the effect of long-term pharmacological interventions including long-term survival studies [21,22]. However, apart from the outstanding cost, the use of animals needs expert skills and long time to yield reliable results. Moreover, the large number of animals are required to make reproducible results, especially in experiments involving pharmacological testing. However, as demonstrated in this study, the use of EHTs is easy, but at the same time, and does not compromise the quality of research outcome. From our experience it is possible to construct more than 5 pieces of EHTs from a single neonatal heart, which give the possibility to test the effect of different pharmacological agents on a single heart preparation. Futhermore, the EHT is useful in reproducing the effects of stresses and pharmacological agents on conduction velocity of action potentials, in a similar way to the whole heart. In addition, as demonstrated in the study, the survival signaling pathway in EHTs responds in a similar way to the whole heart under hypoxic stress.

Taken together, fully developed EHTs exhibit the characteristics of adult hearts and when subjected to hypoxia, they respond identical to the adult myocardium. Although, in vivo experiments are the golden standard for analysis of functional recovery following myocardial injury and pharmacological interventions, the developed EHTs could be used as a replacement for the adult heart in the situation of acute experimental setting, especially for studying the effects of stresses and treatment conduction velocity and molecular expressional changes.

Supporting Information

Figure S1 Mechanical stretch synchronizes the contraction of engineered heart tissue.
Found at: doi:10.1371/journal.pone.0009275.s001 (2.18 MB TIF)

Video S1 Video demonstrating the construction of engineered heart tissue.
Found at: doi:10.1371/journal.pone.0009275.s002 (1.78 MB MP4)

Acknowledgments

We thank Ms. Masayo Yamamoto, Ms. Kayo Okazaki and Ms. Jayanthi Bellae Papannarao for the kind technical assistance in animal maintenance, immunoblotting and cell culture.

Author Contributions

Conceived and designed the experiments: RGK. Performed the experiments: RGK MA. Analyzed the data: RGK. Contributed reagents/materials/analysis tools: RGK YK. Wrote the paper: RGK. Obtained funding for the project: TS.

References

1. Zimmermann WH, Fink C, Kralisch D, Remmers U, Weil J, et al. (2000) Three-dimensional engineered heart tissue from neonatal rat cardiac myocytes. Biotechnol Bioeng 68: 106–114.
2. Zimmermann WH, Melnychenko I, Wasmeier G, Didie M, Naito H, et al. (2006) Engineered heart tissue grafts improve systolic and diastolic function in infarcted rat hearts. Nat Med 12: 452–458.
3. Naito H, Melnychenko I, Didie M, Schneiderbanger K, Schubert P, et al. (2006) Optimizing engineered heart tissue for therapeutic applications as surrogate heart muscle. Circulation 114: I72–78.
4. Zimmermann WH, Schneiderbanger K, Schubert P, Didie M, Munzel F, et al. (2002) Tissue engineering of a differentiated cardiac muscle construct. Circ Res 90: 223–230.
5. Sill B, Alpatov IV, Pacak CA, Cowan DB (2009) Implantation of engineered tissue in the rat heart. J Vis Exp.
6. Migneco F, Hollister SJ, Birla RK (2008) Tissue-engineered heart valve prostheses: 'state of the heart'. Regen Med 3: 399–419.
7. Stevens KR, Kreutziger KL, Dupras SK, Korte FS, Regnier M, et al. (2009) Physiological function and transplantation of scaffold-free and vascularized human cardiac muscle tissue. Proc Natl Acad Sci U S A 106: 16568–16573.
8. Lesman A, Habib M, Caspi O, Gepstein A, Arbel G, et al. (2009) Transplantation of a Tissue-Engineered Human Vascularized Cardiac Muscle. Tissue Eng Part A.
9. Kaully T, Kaufman-Francis K, Lesman A, Levenberg S (2009) Vascularization-the conduit to viable engineered tissues. Tissue Eng Part B Rev 15: 159–169.
10. Katare RG, Ando M, Kakinuma Y, Arikawa M, Handa T, et al. (2009) Vagal nerve stimulation prevents reperfusion injury through inhibition of opening of mitochondrial permeability transition pore independent of the bradycardiac effect. J Thorac Cardiovasc Surg 137: 223–231.
11. Rajesh KG, Sasaguri S, Ryoko S, Maeda H (2003) Mitochondrial permeability transition-pore inhibition enhances functional recovery after long-time hypothermic heart preservation. Transplantation 76: 1314–1320.
12. Ando M, Katare RG, Kakinuma Y, Zhang D, Yamasaki F, et al. (2005) Efferent vagal nerve stimulation protects heart against ischemia-induced arrhythmias by preserving connexin43 protein. Circulation 112: 164–170.
13. Kakinuma Y, Ando M, Kuwabara M, Katare RG, Okudela K, et al. (2005) Acetylcholine from vagal stimulation protects cardiomyocytes against ischemia and hypoxia involving additive non-hypoxic induction of HIF-1alpha. FEBS Lett 579: 2111–2118.
14. Lin JW, Garber L, Qi YR, Chang MG, Cysyk J, et al. (2008) Region [corrected] of slowed conduction acts as core for spiral wave reentry in cardiac cell monolayers. Am J Physiol Heart Circ Physiol 294: H58–65.
15. Rajesh KG, Sasaguri S, Zhitian Z, Suzuki R, Asakai R, et al. (2003) Second window of ischemic preconditioning regulates mitochondrial permeability transition pore by enhancing Bcl-2 expression. Cardiovasc Res 59: 297–307.
16. Katare RG, Zhitian Z, Sodeoka M, Sasaguri S (2007) Novel bisindolylmaleimide derivative inhibits mitochondrial permeability transition pore and protects the heart from reperfusion injury. Can J Physiol Pharmacol 85: 979–985.
17. Akins RE (2002) Can tissue engineering mend broken hearts? Circ Res 90: 120–122.
18. Bailey B, Izarra A, Alvarez R, Fischer KM, Cottage CT, et al. (2009) Cardiac stem cell genetic engineering using the alphaMHC promoter. Regen Med 4: 823–833.
19. Shimizu T, Sekine H, Yamato M, Okano T (2009) Cell sheet-based myocardial tissue engineering: new hope for damaged heart rescue. Curr Pharm Des 15: 2807–2814.
20. Song H, Yoon C, Kattman SJ, Dengler J, Masse S, et al. (2009) Regenerative Medicine Special Feature: Interrogating functional integration between injected pluripotent stem cell-derived cells and surrogate cardiac tissue. Proc Natl Acad Sci U S A.
21. Pfeffer MA, Pfeffer JM, Fishbein MC, Fletcher PJ, Spadaro J, et al. (1979) Myocardial infarct size and ventricular function in rats. Circ Res 44: 503–512.
22. Hasenfuss G (1998) Animal models of human cardiovascular disease, heart failure and hypertrophy. Cardiovasc Res 39: 60–76.

J Physiol Sci (2010) 60:67–74
DOI 10.1007/s12576-009-0071-5

ORIGINAL PAPER

Effect of the cholinesterase inhibitor donepezil on cardiac remodeling and autonomic balance in rats with heart failure

Yoshihisa Okazaki · Can Zheng · Meihua Li · Masaru Sugimachi

Received: 28 July 2009 / Accepted: 4 November 2009 / Published online: 1 December 2009

Abstract In an earlier study we demonstrated the beneficial effect of direct vagal electrical stimulation on cardiac remodeling and survival. In the study reported here, we attempted to reproduce the effect of vagal enhancement through the administration of an acetylcholinesterase inhibitor, donepezil. A rat model of heart failure following extensive healed myocardial infarction was used. Compared to their nontreated counterparts, rats given donepezil (5 mg/kg/day) in their drinking water had a smaller biventricular weight (3.40 ± 0.13 vs. 3.02 ± 0.21 g/kg body weight, $P < 0.05$), and maximal rate of rise (3256 ± 955 vs. 3822 ± 389 mmHg/s, $P < 0.05$) and the end-diastolic value (30.1 ± 5.6 vs. 23.2 ± 5.7 mmHg, $P < 0.05$) of left ventricular pressure were improved. Neurohumoral factors were suppressed in donepezil-treated rats (norepinephrine 1885 ± 1423 vs. 316 ± 248 pg/ml, $P < 0.01$; brain natriuretic peptide 457 ± 68 vs. 362 ± 80 ng/ml, $P < 0.05$), and the high-frequency component of heart rate variability showed a nocturnal increase. These findings indicated that donepezil reproduced the anti-remodeling effect of electrical vagal stimulation. Further studies are warranted to evaluate the clinical usefulness of donepezil in heart failure.

Y. Okazaki · M. Sugimachi
Department of Artificial Organ Medicine, Division of Surgical Medicine, Osaka University Graduate School of Medicine, 2-2 Yamadaoka, Suita, Osaka 565-0871, Japan

Y. Okazaki · C. Zheng · M. Li · M. Sugimachi (✉)
Department of Cardiovascular Dynamics, Advanced Medical Engineering Center, National Cardiovascular Center Research Institute, 5-7-1 Fujishirodai, Suita, Osaka 565-8565, Japan
e-mail: su91mach@ri.ncvc.go.jp

Keywords Heart rate variability · Myocardial infarction · Neurohumoral activation · Vagal stimulation

Introduction

Profound imbalances in the autonomic nervous system, such as overactive sympathetic activity as well as diminished vagal activity, are considered to be important factors that aggravate heart failure [1, 2]. Various therapeutic agents, including beta-blockers [3, 4], angiotensin converting enzyme inhibitors [5, 6], and angiotensin receptor antagonists [7, 8] have proven to be useful pharmacotherapy, not a little by correcting the abnormally augmented sympathetic activity. However, few attempts have been made to date to actively remedy the reduced vagal activity as a treatment for heart failure. As a first attempt to testing this therapeutic strategy, our group has shown that in rats with aggravating chronic heart failure after experimentally induced healed myocardial infarction, electrical stimulation of the vagus nerve markedly improved survival by preventing cardiac remodeling [9].

Since the efferent vagal nerve activity is transmitted by acetylcholine, drugs that increase acetylcholine concentration at the neuro-effector junction are expected to have an effect similar to that of electrical stimulation. In support of this hypothesis, clinical trials in which patients with chronic heart failure were treated with the acetylcholinesterase inhibitor pyridostigmine reported decreased ventricular arrhythmia, enhanced heart rate variability at rest, increased heart rate reserve and oxygen pulse during exercise, and improved heart rate recovery after exercise [10, 11]. However, these studies examined the effect of short-term administration (1–2 days), and to date the long-term effect of pyridostigmine has not been investigated.

Clinical trials have also been conducted on scopolamine, which stimulates vagus nerve centrally at low doses [12, 13]. Transdermal administration of a small dose of scopolamine in patients with heart failure following myocardial infarction was found to increase heart rate variability and enhance baroreflex sensitivity. These studies have not shown, however, an anti-remodeling effect as more direct evidence against the progression of heart failure.

We hypothesized that donepezil, a novel acetylcholinesterase inhibitor, would show various clinically relevant beneficial effects through its preferential effects on neural true cholinesterase (rather than hepatic pseudocholinesterase) [14]. Therefore, in the study reported here, we investigated the effect of donepezil on hemodynamics, neurohumoral activation, and cardiac remodeling in rats with chronic heart failure. We also analyzed the high-frequency (HF) component of the heart rate variability to assess changes in vagal tone [15, 16]. Our results suggest that donepezil reproduces the anti-remodeling effect of electrical stimulation of the vagus nerve and increases vagal tone.

Materials and methods

The protocol of this study was performed in accordance with the Guiding Principles for the Care and Use of Animals in the Field of Physiological Sciences and was approved by the Experimental Animal Committee of the National Cardiovascular Center.

Chronic heart failure model

Male Sprague–Dawley rats (8 weeks of age) were used. A thoracotomy was performed under halothane anesthesia, and the main branch of the left coronary artery was ligated with nylon to produce myocardial infarction. The ligation resulted in myocardial infarction of 45–55%. The rats recovered from this extensive myocardial infarction and progressed to the chronic state of heart failure (see Results). The ventricular fibrillation that occurred within 1 h of ligation was treated actively by defibrillation and cardiac massage in order to salvage as many as possible rats with extensive myocardial infarction.

Experimental protocol

One week after the induction of myocardial infarction, the surviving rats underwent a second operation under halothane anesthesia in which an electrocardiogram (ECG) telemetry device was implanted in each rat to continuously monitor the electrical activity of the heart and heart rate (Fig. 1a).

Rats that survived the second week were divided into a nontreated group and a donepezil group. The donepezil group was administered the acetylcholinesterase inhibitor

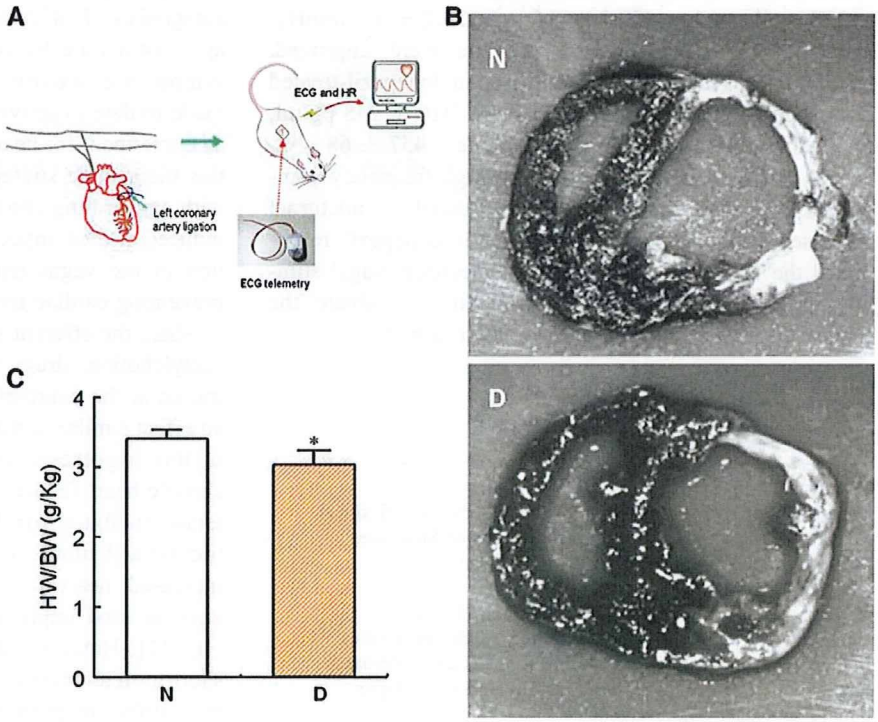

Fig. 1 **a** Schematic representation of the experimental design. Electrocardiogram (*ECG*) was recorded continuously using a telemetric system. **b** Ventricular sections of representative animals at week 6 of treatment (8 weeks post-infarction). No significant difference in the size of the myocardial infarction was observed between the donepezil group and the nontreated group. Compared with the nontreated heart (*N*), the donepezil-treated heart (*D*) had a thicker scar in the infarct area with more spared myocardium in the border area. **c** Combined weight of left and right ventricles per body weight (*HW/BW*) at week 6 of treatment. Ventricular weight was significantly lower ($*P < 0.05$) in the donepezil group (*shaded bar*, *D*) than in the nontreated group (*open bar*, *N*)

donepezil (Aricept; Eisai, Tokyo, Japan) dissolved in drinking water at a concentration of 50 mg/dl. The dose estimated from the volume of water consumed was 5 mg/kg/day on average. The selection of donepezil rested on the fact that, in comparison to other drugs, its inhibition action is directed much more towards the (true) acetylcholinesterase at synapses and effectors and less towards pseudocholinesterase (butyrylcholinesterase) in the liver [14].

At week 6 post-treatment (week 8 after infarction was induced), 13 rats in the nontreated group and 14 rats in the donepezil group were subjected to a hemodynamic study under halothane anesthesia. Following this study and blood collection, the rats were euthanized by an overdose of halothane, and a histological examination was conducted.

In 11 other rats with a similar healed myocardial infarction, the heart rate variability was calculated from the continuous ECG recordings between weeks 12 and 20 post-myocardial infarction induction. Five of these 11 rats served as the nontreated group (weeks 12–20 post-infarction), and six received the donepezil treatment (weeks 17–19 post-infarction). Preliminary analysis indicated no differences in heart rate variability at 8 weeks post-infarction.

Hemodynamic measurement

The hemodynamic study was conducted in rats under halothane anesthesia at week 6 of the treatment period. A Millar catheter (SPC-320; Millar Instruments, Houston, TX) was inserted from the carotid artery into the left ventricle to measure left ventricular pressure (LVP) with a high-fidelity catheter. Based on the LVPs, we calculated the maximal first derivative of left ventricular pressure over time (dP/dt_{max}) and the left ventricular end-diastolic pressure (LVEDP). The right atrial pressure (RAP) was measured by an external transducer via a catheter filled with physiological saline.

Neurohumoral factor measurements

Blood samples (3 ml) were collected and the neurohumoral factors in the blood assayed. As indices of sympathetic activity, norepinephrine (NE) and epinephrine (Epi) were measured by high-performance liquid chromatography with electrochemical detection. The plasma level of brain (or B-type) natriuretic peptide (BNP) was measured by an enzyme-linked immunosorbent (ELISA) assay (BNP-32 Enzyme Immunoassay kit, Peninsula Lab, San Carlos, CA). We included BNP in the assay due to its importance as a strong predictor of prognosis [17, 18]. BNP has been useful in detecting new patients with heart failure and in predicting mortality and cardiac events in both patients and asymptomatic subjects. BNP may also be a useful predictor of heart failure with preserved systolic function.

Heart tissue examination

The left and right ventricles were excised and the total weight measured. Both ventricles were then sectioned into 3-mm-thick slices, starting from the apex towards the base of the heart. Myocardial infarction size was assessed from the proportion of the length of the infarct to the left ventricular perimeter measured on each section.

Power spectral analysis of heart rate variability

The ECG telemetric data were processed as follows. Signals from the transmitter (model TA11CTA-F40; Data Sciences Int, St. Paul, MN) were recorded on a recording software (HEM; Notocord, Newark, NJ). An analysis software program (HRT10a1; Notocord) was used to extract the RR intervals from the data of the continuous recording (1-kHz sampling). All of the RR intervals were extracted from 24-h continuous recording data for the nontreated and the donepezil groups. The text data of 2-h intervals were stored in files to be analyzed later using the heart rate variability analysis software that we developed. Due to the frequent occurrence of extrasystoles in chronic heart failure, it was necessary to develop an original algorithm to process the data, as explained below.

Heart rate variability analysis software

The following procedures were conducted.

1. Data preparation. The 2-h data were combined to obtain 24-h data. The time of R-wave detection and the RR interval were saved as combined data.
2. Removal of extrasystole. A 20-point median filter was applied to all of the RR interval data to produce a sequence. Heart beats with RR intervals differing from the median value by 15 ms (threshold) or above were recognized and recorded as extrasystole or post-extrasystole. These data were excluded from analysis.
3. Resampling of valid interval data. The 24-h data were divided into 6-min data (with 50% overlap). After excluding the RR intervals associated with extrasystole, the valid RR interval data were resampled at intervals of 1/10 s using linear interpolation.
4. Power spectral analysis. In the power spectral analysis, 1024 points of 1/10-s data were grouped into a segment (segment length = 102.4 s) for fast Fourier transformation (FFT). The power spectra obtained from six segments were ensemble-averaged. Prior to FFT, the linear trend was removed from each segment
5. Data selection. Even though extrasystoles are removed, segments with many deleted data cannot be expected to yield reliable power spectral analysis results. Therefore,

data with ≥40 extrasystoles within 6 min were excluded from analysis.

6. Definition of HF component. In this study, the effect of bigeminy that occurs in heart failure was observed in the higher frequency range. Therefore, we excluded frequency range >1.5 Hz, and HF was defined as the power from 0.5 to 1.5 Hz. The power of the HF component was determined during daytime (0600–1800 hours) and nighttime (1800–0600 hours).

Statistical analysis

All data are presented as mean ± standard deviation (SD). Continuous variables were compared using the unpaired *t* test between two groups. The differences were considered significant when $P < 0.05$.

Results

Hemodynamics

Figure 2 shows the measurements of the hemodynamic parameters in rats under anesthesia 6 weeks after the onset of donepezil administration. A LVP waveform and its first derivative (dP/dt) in a nontreated rat are shown in Fig. 2a. Figure 2b shows that the dP/dt_{max} of the nontreated rat was significantly lower than that of the donepezil group (3,256 ± 955 vs. 3,822 ± 389 mmHg/s, $P < 0.05$). The LVEDP and RAP was significantly lowered by donepezil administration compared to the nontreated rat [23.2 ± 5.7 vs. 30.1 ± 5.6 mmHg, $P < 0.05$ (Fig. 2c) and 4.1 ± 2.9 vs. 7.0 ± 4.0 mmHg, $P < 0.05$ (Fig. 2d), respectively]. The contractility index dP/dt_{max} is known as a heart rate-

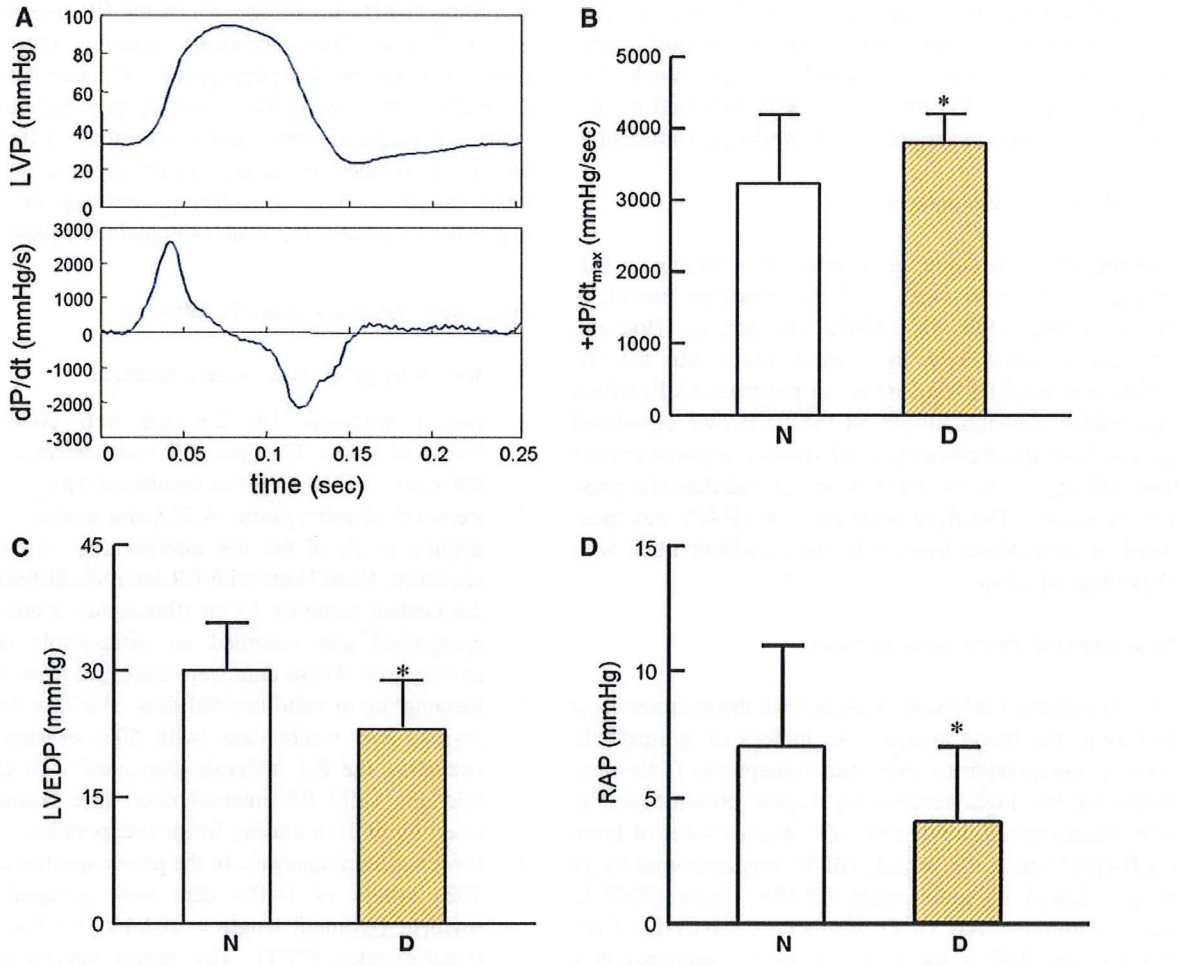

Fig. 2 **a** A representative example of the left ventricular pressure (*LVP*) waveform and its derivative in a nontreated rat. **b** Maximal first derivative of left ventricular pressure (dP/dt_{max}) at week 6 of treatment. The dP/dt_{max} was significantly ($^*P < 0.05$) higher in the donepezil group (*shaded bar*, *D*) than in the nontreated group (*open bar*, *N*). **c** Left ventricular end-diastolic pressure (*LVEDP*) at week 6 of treatment. The LVEDP was significantly lower in the donepezil group (*shaded bar*, *D*) than in the nontreated control group (*open bar*, *N*). **d** Right atrial pressure (*RAP*) at week 6 of treatment. The RAP was significantly ($^*P < 0.05$) lower in the donepezil group (*shaded bar*, *D*) than in the nontreated control group (*open bar*, *N*)